mechanisms underlying molecular motors. There are still many unanswered questions. We need further development of the technique. Different myosins have been discovered according to the development of molecular biology. Combination with protein engineering will be important in future research. The molecular motors are typical molecular machines and the conclusions obtained from the molecular motors will be shared with other molecular machines. The techniques we have developed as well as the knowledge we have acquired will be useful for future studies in the diverse field of bioscience.

We have learned that nanometer-sized protein molecules are influenced by thermal agitation. The input energy level released from the hydrolysis of ATP is the same order as the thermal energy. The measurements that are designed to monitor the behavior of single molecules are influenced by the effect of thermal disturbance. One question arises as to how the protein molecules work efficiently without being disturbed by the effects of thermal motion. Under these circumstances, the protein may harness thermal energy rather than work against thermal disturbance. The single molecule measurements will be tools to deal with thermal fluctuation, which, on the one hand, interferes with the measurements and, on the other hand, drives the function of the molecular machines.

[13] Visualization of Single Molecules of mRNA *in Situ*

By ANDREA M. FEMINO, KEVIN FOGARTY, LAWRENCE M. LIFSHITZ, WALTER CARRINGTON, and ROBERT H. SINGER

Introduction

The purpose of this article is to introduce methods and concepts that facilitate detection and identification of single molecules of mRNA *in situ* using fluorescence *in situ* hybridization (FISH). The methodology employs stringent imaging requirements that include a carefully calibrated quantitative epifluorescence digital imaging microscope, three-dimensional (3D) optical sectioning, constrained iterative deconvolution, and 3D interactive analysis software.[1–3]

[1] R. H. Singer and A. M. Femino, Patent Number 5,866,331. University of Massachusetts, Worcester, 1999.

[2] A. M. Femino, F. S. Fay, K. Fogarty, and R. H. Singer, *Science* **280,** 585 (1998).

[3] A. M. Femino, Doctoral Dissertation, Graduate School of Biomedical Sciences. University of Massachusetts Medical School, Worcester, 2001.

0076-6879/03 $35.00

FISH is a very widely used technique in cell biology. Sensitivity of detection has been the major concern when implementing FISH technology. Previously, probes were designed to maximize signal in order to detect desired genes and transcripts. Large probes such as complete cDNA sequences were labeled with biotin and digoxigenin and detected using fluorochrome-labeled antibodies or streptavidin, respectively, to further amplify the signal.[4–10] Except in cytogenetics, which employed chromosome paints, high background due to nonspecific binding was a drawback and both hampered interpretation and compromised the reliability of information acquired with FISH. Improvements in specificity of FISH came with the use of short DNA oligonucleotide probes conjugated with biotin and digoxigenin.[11–13]

Fluorochrome-Conjugated Oligonucleotide Probes to Facilitate Analysis and Interpretation of FISH Images

Probes based on light emission afford the inherent advantage of accurate spatial detection. The detected signal can in principle be traced back to its source, unlike isotopic emissions that are detected via emulsions frequently at micrometer distances from the source. When a fluorescence signal arises from the fluorochrome molecules that are directly attached to the nucleic acid probe, the target molecule in the specimen can theoretically be located very precisely because the probe hybridizes within angstroms of the target nucleic acid.

The efficacy of using directly fluorochrome-labeled probes as FISH reagents was first tested in our laboratory (Fig. 1).[12,14] The immediate advantage is a one-step process for detection of hybridization sites. A one-step process is desirable because any number of spectrally distinct fluorochromes can be used simultaneously, limited only by the availability of dye molecules with distinguishable excitation and/or emission frequencies, affording detection of greater than two targets simultaneously.

The major disadvantage of fluorochrome-labeled probes is that they pose a detection problem due to their overall diminished intensity, compared to probes

[4] J. B. Lawrence, R. H. Singer, and L. M. Marselle, *Cell* **57,** 493 (1989).
[5] E. Viegas-Pequignot, B. Dutrillaux, H. Magdelenat, and M. Coppey-Moisan, *Proc. Natl. Acad. Sci. U.S.A.* **86,** 582 (1989).
[6] B. F. Brandriff, L. A. Gordon, and B. J. Trask, *Environ. Mol. Mutagen.* **18,** 259 (1991).
[7] B. J. Trask, *Methods Cell Biol.* **35,** 3 (1991).
[8] D. G. Albertson, R. M. Fishpool, and P. S. Birchall, *Methods Cell Biol.* **48,** 339 (1995).
[9] P. S. Birchall, R. M. Fishpool, and D. G. Albertson, *Nat. Genet.* **11,** 314 (1995).
[10] H. Yokota, G. van den Engh, J. E. Hearst, R. K. Sachs, and B. J. Trask, *J. Cell Biol.* **130,** 1239 (1995).
[11] K. L. Taneja and R. H. Singer, *J. Cell. Biochem.* **44,** 241 (1990).
[12] K. L. Taneja, L. M. Lifshitz, F. S. Fay, and R. H. Singer, *J. Cell Biol.* **119,** 1245 (1992).
[13] G. J. Bassell, H. Zhang, A. L. Byrd, A. M. Femino, R. H. Singer, K. L. Taneja, L. M. Lifshitz, I. M. Herman, and K. S. Kosik, *J. Neurosci.* **18,** 251 (1998).
[14] E. H. Kislauskis, Z. Li, R. H. Singer, and K. L. Taneja, *J. Cell Biol.* **123,** 165 (1993).

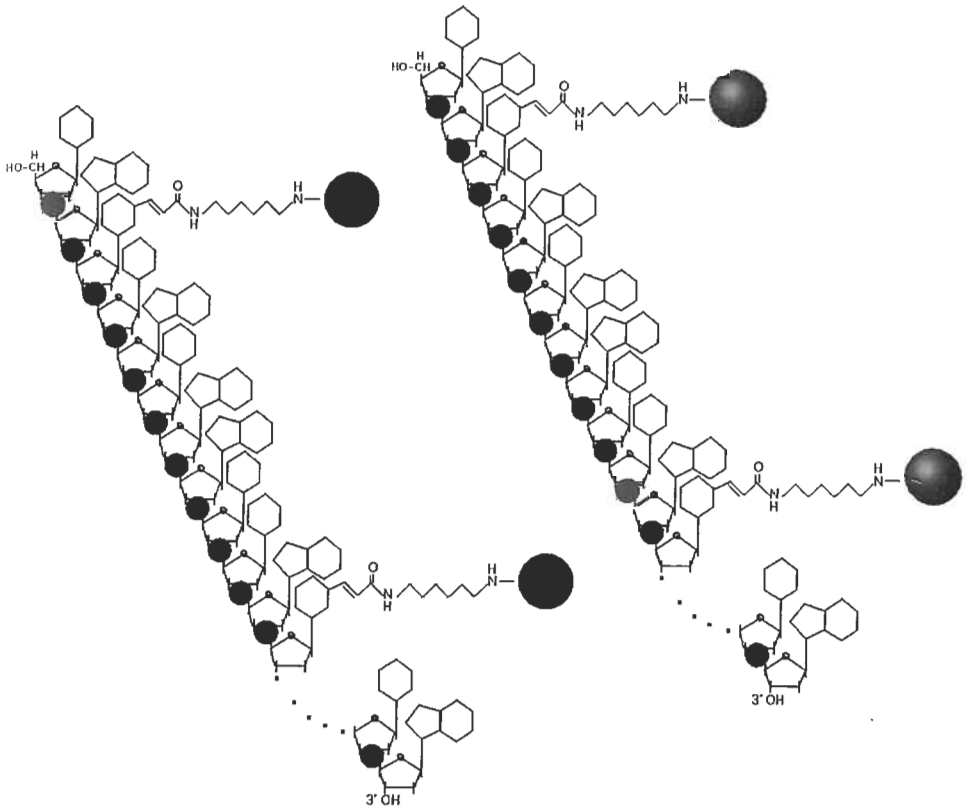

FIG. 1. Fluorochrome-labeled oligonucleotide probes. DNA oligonucleotide probes are specifically engineered to hybridize specific target sequences. A known number of fluorochrome molecules are covalently linked to the modified thymine analogs incorporated in the sequence. The intrinsic TFI of each probe can be calibrated. Many combinations of probes can be hybridized simultaneously.

using secondary detection. Initially species known to be present in high copy numbers such as poly(A) sequences, β-actin mRNA in chicken embryo fibroblasts, and CTG repeats in myotonic dystrophy were detected.[14–19]

An important attribute of the fluorochrome-labeled oligonucleotide probe is the predetermined number of fluorochromes to which it is covalently attached. The

[15] G. Zhang, K. L. Taneja, R. H. Singer, and M. R. Green, *Nature* **372,** 809 (1994).
[16] K. L. Taneja, M. McCurrach, M. Schalling, D. Housman, and R. H. Singer, *J. Cell Biol.* **128,** 995 (1995).
[17] D. A. Samarsky, M. J. Fournier, R. H. Singer, and E. Bertrand, *EMBO J.* **17,** 3747 (1998).
[18] J. C. Politz, R. A. Tuft, T. Pederson, and R. H. Singer, *Curr. Biol.* **9,** 285 (1999).
[19] H. L. Zhang, R. H. Singer, and G. J. Bassell, *J. Cell Biol.* **147,** 59 (1999).

probe provides a constant measurable signal and becomes amenable to calibration. Calibrated probes provide accurate intensity information and facilitate a definitive analysis of the fluorescence distribution in a FISH image in terms of number of probes hybridized.

Single Molecule Detection Feasible for Wide-Field Epifluorescence Microscopy

The feasibility of detecting and identifying specific single mRNA molecules with state of the art FISH and conventional light microscopy had not been entertained by those closely involved with *in situ* hybridization techniques even with the advent of digital imaging microscopy.[20] Previous detection of single mRNA molecules *in situ* was done by electron microscopy (EM).[21]

A very important finding was that with current digital imaging technology, there is adequate sensitivity to detect single probes *in situ* linked to as few as three to five fluorochromes using conventional epifluorescence microscopy.

Importance of Methodology

The methodology has made it possible to detect and identify a single molecule of mRNA in three-dimensional space, *in situ*, by applying a systematic approach to identify true hybridization signals.

The importance of having the ability to detect single molecules is highlighted by the interest and efforts of many investigators. In other laboratories implementation of single molecule detection has been accomplished under controlled experimental conditions that guarantee single molecules *in vitro* while employing highly specialized microscopic methods for detecting and studying those molecules.[22–26] In contrast, the methodology described here allows the identification of uncharacterized single molecules *in situ* in three-dimensional (3D) space through the analysis of the total fluorescent intensity (TFI) of hybridization sites.

Quantitative Epifluorescence Digital Imaging Microscope with Optical Sectioning

Development of Digital Imaging Microscope

3D digital imaging microscopy employing a conventional epifluorescence microscope with image deconvolution was a novel technology into the early 1990s

[20] D. M. Shotton, *Histochem. Cell Biol.* **104,** 97 (1995).
[21] G. J. Bassell, C. M. Powers, K. L. Taneja, and R. H. Singer, *J. Cell Biol.* **126,** 863 (1994).
[22] K. Peck, L. Stryer, A. N. Glazer, and R. A. Mathies, *Proc. Natl. Acad. Sci. U.S.A.* **86,** 4087 (1989).
[23] E. Betzig and R. J. Chichester, *Science* **262,** 1422 (1993).
[24] J. K. Trautman, J. J. Macklin, L. E. Brus, and E. Betzig, *Nature* **369,** 40 (1994).
[25] S. Nie, D. T. Chiu, and R. N. Zare, *Science* **266,** 1018 (1994).
[26] T. Funatsu, Y. Harada, M. Tokunaga, K. Saito, and T. Yanagida, *Nature* **374,** 555 (1995).

primarily limited to only a few laboratories. The 3D optical sectioning microscope was first described in the literature by Agard and Sedat.[27,28] Images were acquired as standard microphotographs that required digitization so that they could be deconvolved.

3D optical sectioning with deconvolution became more feasible with the advent of the charge-coupled device (CCD) cameras. The late Fredric S. Fay, with colleagues at the Biomedical Imaging Facility, located at the University of Massachusetts Medical School, developed a computerized digital imaging microscope (DIM).[29,30]

The availability of DIM for general research was a major contributor to the success of the work described in this article. The imaging station was optimized for low-light level and high-resolution imaging, which proved to be adequate for the detection and visualization of single molecules *in situ* as described in this work.

A Photometrics Series 180 back-thinned cooled CCD had high quantum efficiency (QE), 80% at peak wavelength, that increased the signal for any given illumination compared to standard front acquisition CCDs. The higher sensitivity reduced the requirement for longer exposures, which in turn reduced fading of fluorescent probes. The cooled CCD (−40.5°) allowed integration of signal without increasing the dark current significantly. Integration times were adjusted to improve the signal-to-noise (*S/N*) ratio in a read noise (50 e^- RMS at 50-kHz readout rate) limited system. The CCD camera was attached to a modified Nikon epifluorescence inverted microscope under computer control. The microscope was equipped with a stepping motor and eddy current sensor that provided accurate change of focus with 100 nm per step and a 100-W mercury lamp. The functions required to image a fluorescent specimen with optical sectioning were precisely synchronized under computer control.

The quantitative and spatial accuracy of fluorochrome-labeled oligonucleotide probes can best be used to advantage with a CCD detection system. The use of a CCD camera provides a sensitive, linear, detection method to capture emitted photons quantitatively onto a high-resolution pixel array. The photon energy, which is converted to a digital signal and further amplified quantitatively, becomes amenable to further quantitative processing and analysis.

General information about CCD cameras, including important considerations concerning their practical application to low-light imaging, can be found in "Methods in Cell Biology: Video Microscopy."[31]

[27] D. A. Agard and J. W. Sedat, *Nature* **302,** 676 (1983).
[28] D. A. Agard, *Annu. Rev. Biophys. Bioeng.* **13,** 191 (1984).
[29] F. S. Fay, K. E. Fogarty, and J. M. Coggins, *in* "Optical Methods in Cell Physiology" (P. D. Weer and B. Salzberg, eds.), p. 51. John Wiley & Sons, New York, 1986.
[30] F. S. Fay, W. Carrington, and K. E. Fogarty, *J. Microsc.* **153,** 133 (1989).
[31] G. Sluder and D. E. Wolf, eds., *Methods Cell Biol.* **56** (1998).

Quantitative Fluorescence Microscopy: An Important Tool in Cell Biology

With the advent of digital imaging, quantitative fluorescence microscopy became a sophisticated, high-performance technique by 1994, with broad applications.[32–36] The commercial availability of high-quality objective lenses and sensitive, cooled CCDs is credited for the major improvements in sensitivity, spatial resolution, and quantitative capability of conventional fluorescence microscopy.[37–39]

Three-dimensional applications using digital imaging microscopy have diversified considerably since the pioneering work of Fay and Agard, due to commercially available and affordable digital image microscopes and powerful computer processors.[40] Countless structures and biological constituents have been visualized for their spatial, temporal, and quantitative distribution *in situ*. Visualization of single genes, specific mRNAs, structural proteins, and transient pulses of chemical messengers such as calcium ions is described in the current literature.[41–44]

The importance of digital images stems from their potential to represent light emissions from biological specimens in terms of accurate numerical data. The numerical data can be further processed to extract quantitative information concerning the functions of cells and their cellular components. The majority of published works to date utilized relative fluorescence intensities emitted from an interrogated single cell to quantify and compare levels of cellular components or to define the spatial boundaries of objects of interest. Image analysis approaches have been highly customized to meet the specific needs of diverse experiments.

[32] G. R. Bright, *in* "Fluorescent Probes for Biology Function of Living Cells—A Practical Guide" (W. T. Mason and G. Rolf, eds.), p. 204. Academic Press, New York, 1993.

[33] D. L. Taylor and Y. L. Wang, "Fluorescence Microscopy of Living Cells in Culture." Academic Press, San Diego, CA, 1989.

[34] A. Waggoner, R. DeBiasio, P. Conrad, G. R. Bright, L. Ernst, K. Ryan, M. Nederlof, and D. Taylor, *Methods Cell Biol.* **30,** 449 (1989).

[35] B. Herman and J. J. Lemasters, "Optical Microscopy: Emerging Methods and Applications." Academic Press, San Diego, CA, 1993.

[36] C. V. Johnson, R. H. Singer, and J. B. Lawrence, *Methods Cell Biol.* **35,** 73 (1991).

[37] Y. Hiraoka, J. W. Sedat, and D. A. Agard, *Science* **238,** 36 (1987).

[38] R. S. Aikens, D. A. Agard, and J. W. Sedat, *Methods Cell Biol.* **29,** 291 (1989).

[39] M. Coppey-Moisan, J. Delic, H. Magdelenat, and J. Coppey, *Methods Mol. Biol.* **33,** 359 (1994).

[40] R. Rizzuto, W. Carrington, and R. A. Tuft, *Trends Cell Biol.* **8,** 288 (1998).

[41] R. M. Long, R. H. Singer, X. Meng, I. Gonzalez, K. Nasmyth, and R.-P. Jansen, *Science* **277,** 383 (1997).

[42] G. J. Bassell, H. Zhang, A. L. Byrd, A. M. Femino, R. H. Singer, K. L. Taneja, L. M. Lifshitz, I. M. Herman, and K. S. Kosik, *J. Neurosci.* **18,** 251 (1998).

[43] K. L. Taneja, L. M. Lifshitz, F. S. Fay, and R. H. Singer, *J. Cell Biol.* **119,** 1245 (1992).

[44] F. S. Fay, K. L. Taneja, S. Shenoy, L. Lifshitz, and R. H. Singer, *Exp. Cell Res.* **231,** 27 (1997).

Theoretical Basis of This Work

The following discussion is undertaken to provide an overview of some basic theoretical concepts in digital image processing that provide a theoretical foundation for quantitative imaging. Image formation theory that encompasses concepts relevant to single molecule detection will be highlighted.

The limitations of optical microscopy are reviewed to emphasize the need for optical sectioning and rigorous deconvolution algorithms to restore images to their true point source distributions. Deconvolution facilitates quantitative analysis of fluorescence distributions, especially in biological specimens with 3D distribution of multiple targets.

Formation of a Digital Image Described Mathematically

The basic principles of digital imaging were developed and described in great detail before the application to microscopy.[45,46]

The definition of an image takes on two forms. The true image, i.e., the input image, is comprised of point sources at specific locations in a sample. The output or actual observed image, however, is a distorted version of the input image, and is dependent on the optical properties of the imaging microscope and detector. A major source of distortion of the input image is the diffraction limited optics of a light microscope. For many purposes the observed image suffices to provide necessary information about the outcome of an experiment. It is possible, however, to solve for the true image using a mathematical approach. For the successful interpretation of 3D FISH images with single molecule accuracy it is necessary to solve for the true image.

A mathematical description for the generation of a fluorescence image by a quantitative fluorescence microscope begins with a test point, i.e., a point source with a spatial location, unit intensity, and no spatial extent. This point source is considered a unit impulse $\delta(x, y)$ and is defined such that its total brightness is one.[47]

$$\begin{aligned} &\delta(x, y) = 0 \qquad \text{unless } x = y = 0 \\ &\int_{-\infty}^{\infty} \int_{-\infty}^{\infty} \delta(x, y)dx\, dy = 1 \end{aligned} \tag{1}$$

The point source by definition is located at the origin of the x, y coordinate system, therefore only at coordinates $x = y = 0$ is the delta function nonzero. The

[45] K. R. Castleman, *in* "Digital Image Processing" (A. V. Oppenheim, ed.), p. 429. Prentice-Hall, Englewood Cliffs, NJ, 1979.

[46] K. R. Castleman, *in* "Digital Image Processing," p. 667. Prentice Hall, Upper Saddle River, NJ, 1996.

[47] I. T. Young, *Methods Cell Biol.* **30,** 1 (1989).

total brightness of the point source at $x = y = 0$ is 1. Therefore, integrated over all two-dimensional space, the total brightness of the point source is still 1, since the unit impulse contributes zero brightness to all other coordinates in 2D space.

Equation (1) states a basic and key premise in fluorescence digital imaging microscopy: light emanates from infinitely small point sources. Image processing can then also be based on the theory of image formation by point sources without spatial dimensions.

Images of cells interrogated with fluorescent probes are composed of point sources as well as extended sources. With the added concept of a linear, shift invariant system any light source can be thought of as a superposition of point sources. Extended sources can then also be modeled as a superposition of point sources. Shift invariance means that the intensity information from any point source in the input image must not be dependent on position. The objective lens and detector are the most critical components for this attribute. In a linear imaging system the relative brightness among the multitude of point sources does not change as the light traverses the optical system and is detected on a CCD array or other detector. The absolute intensity, however, of the point sources can be expected to change due to various sources of light loss, but that will not affect the relative weighting of the point spread functions.

Equations (2) and (3) describe the formation of an image.[47] A collection of unit impulses at different positions in a sample with weighting coefficients $a(u, v)$ can produce an arbitrary input image $a(x, y)$.

Input image:

$$a(x, y) = \int_{-\infty}^{\infty} \int_{-\infty}^{\infty} a(u, v)\delta(x - u, y - v)du\,dv \tag{2}$$

The output image is dependent on the mode of detection of the input image. Each weighted input impulse, $a(u, v)\delta(x - u, y - v)$, when imaged through a microscope, generates a weighted point spread function $a(u, v)h(x - u, y - v)$. The sum of the weighted point spread functions is the resulting output image $b(x, y)$.[47]

Output image:

$$b(x, y) = \int_{-\infty}^{\infty} \int_{-\infty}^{\infty} a(u, v)h(x - u, y - v)du\,dv \tag{3}$$

The input image $a(x, y)$ produces an output image described mathematically as $b(x, y)$ only if an imaging system is both linear and shift invariant.

Point Spread Function

In Eq. (3), $h(x, y)$ represents the output image produced by a single point source of light and is referred to as the point spread function (PSF). The PSF

contains all of the information necessary to describe the imaging system, which leads to the convolution Eq. (4).[47] Equation (4) is frequently encountered but is just another way of writing Eq. (3).

$$b(x, y) = a(x, y)^* h(x, y) \tag{4}$$

The output image $b(x, y)$ is described as the product of convolution between $a(x, y)$, the true distribution of input impulses, and the output image $h(x, y)$, referred to as the PSF formed by a single input impulse or point of light. The output image $h(x, y)$, is a distorted description of a true undistorted point source with zero spatial dimensions and contains all the information necessary to describe the imaging system.

The nature of the imaging process causes distortions in the input image as it passes through the optical system. An image of a 3D PSF that is obtained under identical imaging conditions as a FISH image (identical coverslip thickness, mounting media, wavelength, optical setup) contains all the information necessary to describe the optical setup to deconvolve the respective FISH image. Aberrations and asymmetries along the optical axis as well as the diffraction pattern of in and out of focus light all contribute to producing the 3D PSF. The 3D PSF completely describes the behavior of a point source in 3D, assuming a linear, shift-invariant system.

When an accurate description of $h(x, y)$ is available, for example, when an empirical PSF for an imaging setup has been obtained, the output $b(x, y)$ for any other input image $a(x, y)$ can be computed through the process of convolution [Eq. (4)]. Therefore one can simulate an output image, as it would appear through a particular optical system from any model-input image. In fact, this same process is used by deconvolution algorithms to solve for the input image $a(x, y)$ of an unknown fluorescence distribution. In essence, an input image $a(x, y)$ is estimated and then convolved with the PSF. The resulting attempt at simulating the output image $b(x, y)$ is compared to the actual empirical output image. When the difference between the simulated output image and the empirical output image converges, the image is said to be deconvolved or solved for the true input image $a(x, y)$, because convolving the PSF with this estimated input image $a(x, y)$ in fact produces the empirical output image $b(x, y)$.

Successful deconvolution is dependent on obtaining a PSF of high quality. A desirable PSF is one that has good signal-to-noise (S/N) ratio at the plane of focus and at out of focus planes. The in-focus plane should have equal numbers of out of focus planes above and below. The number of optical sections in the PSF should be equal to at least twice that of an image that will be deconvolved (Fig. 2).

A typical cultured cell 5 μm in thickness will require from 20 to 50 optical sections to go out of focus above and below the cell using 0.250 or 0.100 μm z-steps, respectively. The respective PSF must use the same z-step and have 41 to 101 planes, respectively. The most distant planes have expanded diffuse rings and loss

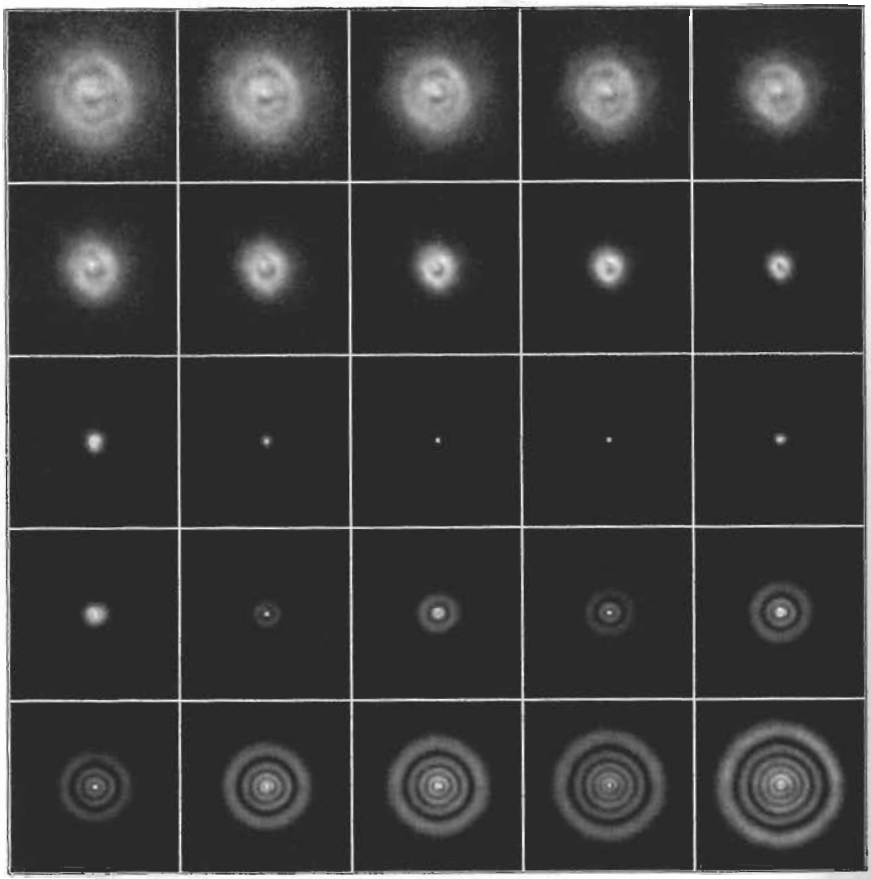

FIG. 2. A 199-nm red fluorescent bead (Molecular Probes) has sufficient intensity to acquire a PSF with good *S/N* ratio 50 planes above and 50 planes below the in-focus plane. The PSF is imaged with a Photometrics Series 200 back thinned camera on an Olympus AX70 upright epifluorescence microscope with a 60× infinity corrected objective, 1.4 NA, 4× camera eyepiece at wavelength 585 nm. The xy pixel size is 100 × 100 nm and the z step = 100 nm. Every fourth plane from a total 100 planes is depicted. The maximum intensity pixel in the in-focus plane (center panel) is 10,852 out of a possible 16,384 (66% of the dynamic range). The individual panels are autoscaled to view the dim rings.

of intensity per pixel, which reduces the *S/N*. A PSF acquired with a wide dynamic range 14-bit CCD camera that has a gray scale from 0 to 16,384 can use adequate exposure times to increase the *S/N* of the out of focus rings without saturating the pixels at the plane of focus. A PSF acquired with a 12-bit CCD camera that has a gray scale from 0 to 4096 will have less dynamic range to have good *S/N* for the out of focus rings without saturating the CCD with light in the plane of focus. A PSF

taken with a variable exposure time, increasing exposure as one moves away from the focal plane, can overcome this limitation. The maximum intensity pixel in the plane of focus should not be greater than 85% of the full dynamic range of the camera: 3482 for a 12-bit vs 13,926 for a 14-bit CCD camera.

FISH Image

A FISH image is a record of the spatial coordinates of one or multiple copies of fluorescent probe molecules by virtue of their fluorescence emission. Their respective target molecules determine the exact locations of the probe molecules, in 3D space.

The fluorescence emitted from point sources is distorted due to resolution limitations of a diffraction-limited microscope. The resulting distorted image may appear to have "objects" with volume, shape, and surface boundaries. Objects will generally have poorly demarcated edges, especially when the signal is weak. The hazy appearance of objects and their boundaries masks the true collection of point sources that is producing the image.

To extract maximum information from an image, the technical limitations of lenses and *S/N* must be understood and optimized. The remainder of this section will highlight the limitations of optics and the need for deconvolution to improve resolution.

Diffraction-Limited Light Microscopy

The image of a point source of light formed in the focal plane of a converging lens is not a point. This is because a light microscope produces diffraction-limited images. The image is a circular diffraction pattern, which appears as a circular disk surrounded by progressively fainter secondary rings. This image of a point source is referred to as an Airy disk.[48] The image of a point source in an image plane is also referred to as a two-dimensional (2D) PSF. Any asymmetries in the ring pattern are related to illumination conditions and aberrations in the objective lens. A 3D PSF may include asymmetries in the cone rings that reflect mismatches in the refractive index between objective lens, coverslip, and mounting medium.

Two point sources whose images partially overlap but are located in the same focal plane can be resolved. Theoretically, the x, y positions of the respective point sources can be measured to 10 nm precision using the symmetry information in the diffraction pattern or using center of mass calculations.[49,50] Point

[48] D. Halliday and R. Resnick, *in* "Physics for Students of Science and Engineering," Combined Ed., p. 1020. John Wiley & Sons, New York, 1965.
[49] S. Inoue, *Methods Cell Biol.* **30,** 85 (1989).
[50] J. L. Harris, *J. Opt. Soc. Am.* **54,** 931 (1964).

sources in thin specimens (200 nm) are amenable to such precision measurements because out of focus light is minimized and image contrast can be sufficiently optimized.

Intensity Information in Focal Plane as Summation of In-Focus as Well as Out-of-Focus Signal

Thicker specimens such as cultured cells and thin tissue sections present a problem when using a conventional fluorescence microscope at high magnifications because of the small depth of focus.[39] Molecular targets detected by fluorescent probes will in all probability occur in 3D spatial distributions in thicker specimens (>200 nm).

The formula for depth of focus, DF, is

$$DF = \frac{100}{7NAM_1} + \frac{\lambda}{2NA^2} \tag{5}$$

The parameters are the wavelength of illumination, λ, in micrometers, the total magnification, M_1, and the numerical aperture of the objective lens, NA. The resulting DF is expressed in micrometers. For a magnification of 300× and $NA = 1.4$ the depth of focus is 0.16 μm for a wavelength of 500 nm (Table I).

A typical cultured cell has a thickness equal to 5.0 μm. When viewing one optical section through a cell those objects that are in the focal plane or out of that focal plane by less than or equal to the DF are visualized with clarity. Structures just outside the DF are visible but blurred due to the 3D PSF that expands the total fluorescence intensity of a point source into peripheral rings thus diminishing the central intensity that demarcates the x and y coordinates of the point source. Structures at greater distances above and below the plane of focus are not

TABLE I
DEPTH OF FOCUS (DF) AS A FUNCTION OF TOTAL MAGNIFICATION, NUMERICAL APERTURE (NA), AND EMISSION WAVELENGTH (λ)[a]

Objective	Camera eyepiece	NA	DF (μm)				μm/pixel[b]
			λ(0.450)	λ(0.520)	λ(0.585)	λ(0.667)	
100×	2.5×	1.4	0.156	0.173	0.190	0.211	0.112
100×	5.0×	1.4	0.135	0.153	0.170	0.191	0.056
100×	2.5×	1.3	0.177	0.198	0.217	0.241	0.112
100×	5.0×	1.3	0.155	0.176	0.195	0.219	0.056
60×	2.5×	1.4	0.183	0.201	0.217	0.238	0.187
60×	5.0×	1.4	0.149	0.167	0.183	0.204	0.093

[a] The wavelength and DF are given in micrometers.
[b] The pixel dimensions at the specimen focal plane of the DIM optical setup used in this work are also listed for the record.

visible because the central intensity disappears but out of focus light from the same structures reaches the focal plane as diffuse rings and immerses objects in the focal plane in a haze or glow. Therefore, any one individual plane cannot provide a complete unambiguous interpretation of structures or events occurring in single cells or in thin tissue sections.

More importantly the accuracy of any measurement of TFI associated with low-light level objects such as single molecules is compromised. Hybridized molecular targets located throughout the spatial volume of cultured cells and tissue sections may contribute fluorescence from planes above and below the focal plane confounding the resolution of point sources in any one focal plane. Contributions from out of focus light are additive, decrease contrast, and preclude the unambiguous assignment of Airy disk patterns to individual point sources. This becomes problematic for determination of TFI attributed to any one point source and is incompatible with single molecule analysis.

Precise Optical Sectioning

The information in a 3D cell or tissue section can be more accurately determined if a number of different focal planes through the specimen are imaged and then examined jointly with the information reconstructed to display the total 3D view from the individual planes (Fig. 3).

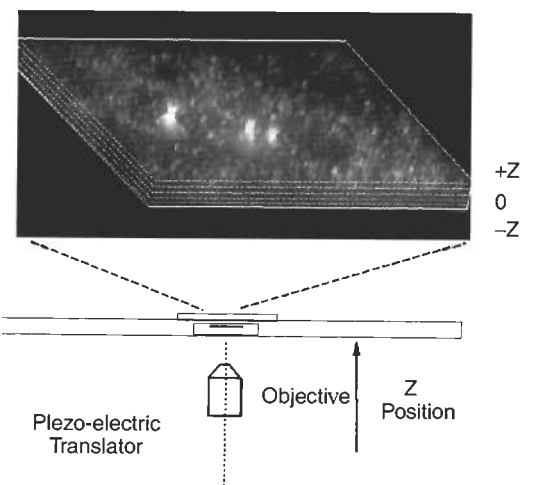

FIG. 3. Optical sectioning produces a stack of sequential two-dimensional images referred to as a 3D stack. Each 2D image contains both in focus and out of focus fluorescence intensity information. The image is viewed through the 2D stacks as a 3D rendering. A bright 100-nm fluorescent bead is at the left and two transcription sites are located near the center of the image. Single molecules of mRNA are seen as dim point sources immersed in the haze of out of focus light.

Optical sectioning provides a nondestructive process for viewing and documenting the fluorescence distribution of a specimen at different depths with incremental steps as small as 100 nm. The fluorescence signal is imaged and digitized at each step along the optical axis as a 2D image. The stack of sequential 2D images, referred to as a 3D stack, contains both in focus as well as out of focus information.

Previously an input image was described as a 2D distribution of weighted point sources. This model also holds true in the present case, but because the point sources are distributed throughout 3D space, an input image must be described at multiple optical planes to document the 3D spatial distribution of point sources and their respective intensity distributions.

The mathematical notation for optical sectioning based in a Cartesian coordinate system is described in Castleman and clarifies the notation that is used to describe deconvolution.[51] If two conditions are met, (1) the specimen function $f(x, y, z)$ is zero outside the field of view in x and y, i.e., the specimen is an isolated single cell and all point sources that contribute signal are located in the imaged field or within the cell boundaries, and (2) the function is zero outside the range $0 \leq z \leq T$, i.e., the optical sectioning went both above ($> T$) and below (< 0) the boundaries of the specimen, then the output image $g(x, y, z')$ can be described as a 3D convolution of the specimen function $f(x, y, z)$, the true fluorescence distribution, with a 3D PSF of the optical system.[51] There is adequate information in the 3D output image, $g(x, y, z')$, to determine the location of point sources of light, i.e., to solve for $f(x, y, z)$.

Deconvolution: An Indispensable Image Processing Step

What approaches can be used to recover the 3D specimen input function $f(x, y, z)$ from the series of output images $g(x, y, z')$ that are distorted by out of focus haze and other aberrations of the optical system?

The process of recovery of the unperturbed input image $f(x, y, z)$ is referred to as a deconvolution, restoration, or reconstruction.[51] Deconvolution will be the term used. The approach most important to this work is the constrained iterative deconvolution. A synthetic specimen function is deconvolved through an iterative process such that when this same function is blurred with the 3D PSF of the optical setup, the result yields approximately the recorded image of the actual biological specimen. The process of the constrained iterative deconvolution is to start with an initial approximation of the specimen function, $f_0(x, y, z)$, and determine the error, $e_i(x, y, z)$, that remains after the ith iteration,

$$e_i(x, y, z) = g(x, y, z) - [f_i(x, y, z)^* h(x, y, z)] \tag{6}$$

where $f_i(x, y, z)$ is the ith approximation of the specimen function, $g(x, y, z)$

[51] K. R. Castleman, *in* "Digital Image Processing," p. 566. Prentice-Hall, Upper Saddle River, NJ, 1996.

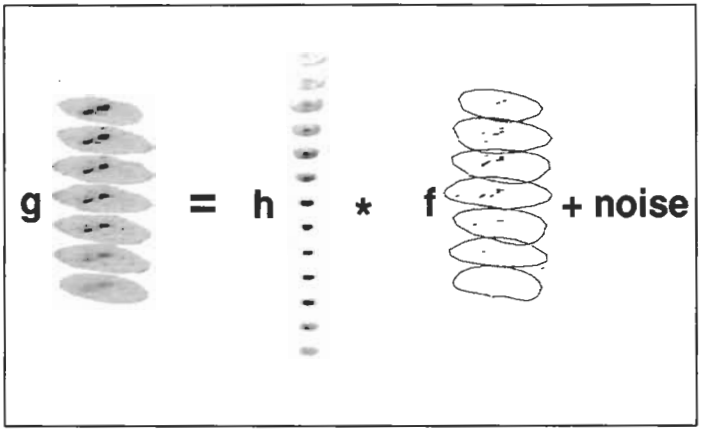

FIG. 4. Noise is a random component of a digital image. The empirical image (g) is formed by convolution of the input image (f) with the PSF (h) of the optical setup and includes random noise from the output electronics of the detector.

is the recorded image, $h(x, y, z)$ is a known 3D PSF, and * is convolution.[52] After each iteration, the ith approximation of the specimen function $f_i(x, y, z)$ is convolved with the 3D PSF. The product of the convolution is compared to the output image function $g(x, y, z)$ and the difference recorded as the error function $e_i(x, y, z)$. A correction is then made to $f_i(x, y, z)$ by some process based on the error function. A unique solution is arrived at when the system converges, a state where further changes in $f_i(x, y, z)$ do not improve the approximation evidenced by the error function. Accuracy of the solution is improved when more constraints are imposed on the solution. A common constraint is that the specimen function must be nonnegative. This is a very reasonable constraint for fluorescence images because fluorescent signal is intrinsically nonnegative.

The 3D imaging process is a blurring process with additional noise components introduced after blurring (Fig. 4). The noise comes primarily from the electronics. Such noise components do not correspond to any possible specimen components. Noise is a random contribution and will not form any consistent blurring pattern as would true point sources located in the specimen. Therefore noise in the final image $g(x, y, z)$ will confound any solution. The noise contribution must be remedied in order to converge to a unique and accurate solution.

A "well-posed" approximation is one that does have a unique solution and is not sensitive to the presence of noise.[53] Such a process is the constrained iterative

[52] K. R. Castleman, *in* "Digital Image Processing," p. 574. Prentice-Hall, Upper Saddle River, NJ, 1996.

[53] W. Carrington, *Proc. SPIE* **1205,** 72 (1990).

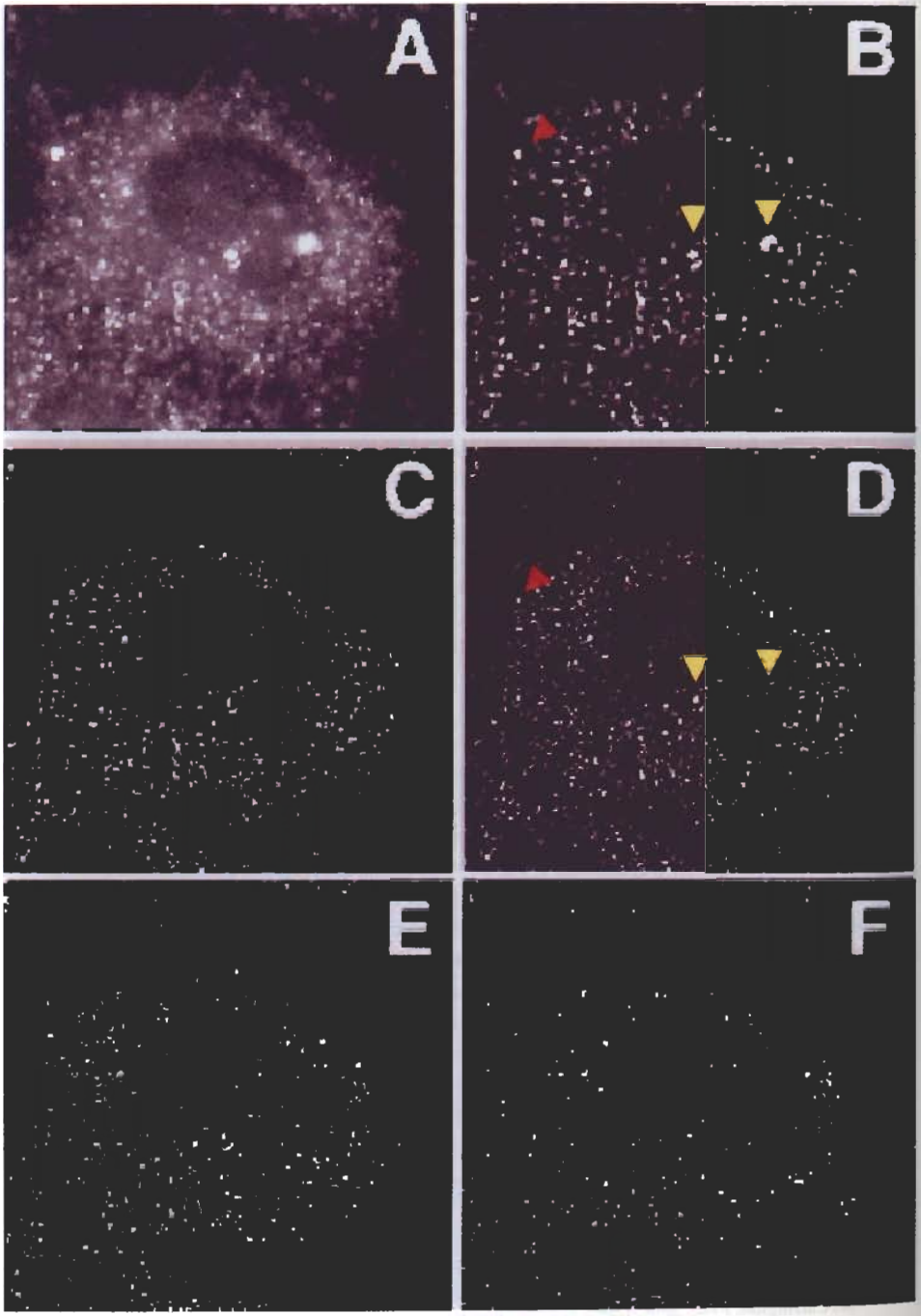
A
B
C
D
E
F

regularization procedure that seeks a solution that approaches the true input fluorescence distribution as the noise is reduced and as the image is sampled more finely and over a larger volume.[53] The regularization seeks a function $f(x, y, z)$ that minimizes the error function $e_i(x, y, z)$

$$e_i(x, y, z) = \sum_{i,j,k} | g_{ijk} - [f(x, y, z)^* h]_{ijk} |^2 + \alpha \iiint | f(x, y, z) |^2 \, dx \, dy \, dz \tag{7}$$

The function $f(x, y, z)$ is the nonnegative function that simulates the specimen function.[53] The second term on the right side of the equation enforces smoothness on $f(x, y, z)$ to prevent noise in g_{ijk} from introducing oscillations that would corrupt the solution for an accurate $f(x, y, z)$. When a large α value such as 10^{-3} is chosen, the solution is allowed to converge with a larger error function $e_i(x, y, z)$. When a small α value such as 5×10^{-6} is chosen, the soultion does not converge until a smaller error function $e_i(x, y, z)$ can be attained, which usually requires a greater number of iterations and increased processing time. The α parameter is adjusted to optimize the minimization process of Eq. (7). Optimization is here defined as a set of conditions that allows the iterative process to converge with a minimal error function $e_i(x, y, z)$ within a reasonable time without compromising the accuracy of the solution (Figs. 5 and 6). The selected α value is too small when it becomes incompatible with the level of random noise inherent in the empirical image $g(x, y, z)$ and the process cannot converge. Residuals are reported for a completed deconvolution and represent the percent of signal that could not be reassigned. The expected residuals for a given optical setup can be estimated.

Exhaustive photon reassignment (EPR) is the name given to the patented iterative numerical method for minimization of Eq. (7) published by Walter Carrington.[53] Work described in this article uses EPR exclusively. The EPR algorithm is broadly applicable to a wide range of image types.

FIG. 5. A deconvolution using EPR approaches the best solution when an image converges with the minimum of residuals that can be expected for the noise level of the system. (A) Raw image of a cell hybridized with a CY3 probe to the 3′-UTR of β-actin RNA. The image is deconvolved using a variety of α-values (B–F). A solution is achieved using α-values between 1E-05 and 5E-06 (D and E). As the deconvolution approaches a solution the fiduciary 100-nm bead (red arrow) condenses to a point source. The transcription sites (yellow arrows) become less visible, which indicates that they are located deeper in the nucleus and we are observing their out of focus light in (B) The α-value, number of iterations achieved, convergence achieved (convergence is set at 0.001), and percent residuals are listed for (B)–(F): (B) 0.001, 64, 0.000915, 15.3; (C) 0.0001, 153, 0.000932, 11.0; (D) 1E-05, 321, 0.000974, 10.2; (E) 5E-06, 395, 0.0014, 10.2; (F) 1E-06, 400, 0.0303, 10.6. The α-value of 1E-06 (F) did not allow the image to converge within a reasonable number of iterations and therefore is assumed to be a limit to any practical improvement of the result. Pixel dimensions are $x = 187$ nm, $y = 187$ nm, $z = 250$ nm.

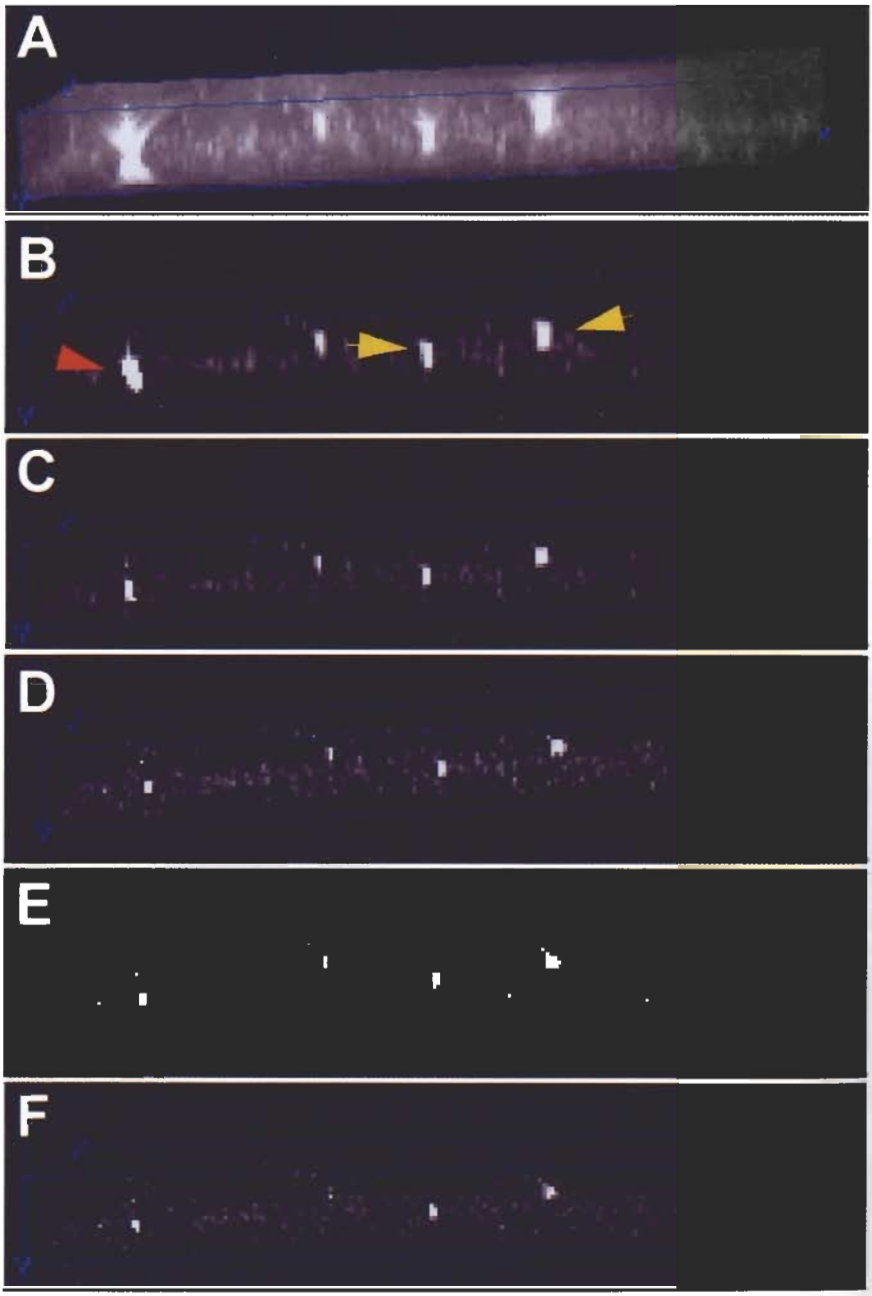
A
B
C
D
E
F

A very important aspect of the constrained iterative regularization algorithm, fundamental to the success of the work described in this article, is its quantitative accuracy. The EPR algorithm maintains the total intensity of the image as it approaches the best solution. The restoration process accounts for the total signal that is attributed to each point source. All the out of focus light, attributed to a particular point source, from above and below the plane of focus is returned to the plane of focus within the limits of resolution. The number of planes in the PSF determines the depth from which out of focus light is returned to each point source in the experimental image. To ensure that a point source, located in the highest or lowest optical plane of the experimental image, can be deconvolved accurately the number of planes on either side of the PSF focal plane must equal the number of planes in the experimental image.

The nonnegative constraint on the iterative method also leads to the possibility of resolution beyond the diffraction limit. Improved resolution is evidenced by a decrease in the full-width at half-maximum intensity of the image of a fluorescein-labeled 200-nm bead from 0.32 to 0.23 μm in the x and y dimension and 0.79 to 0.57 μm along the z axis.[54]

A version of EPR running on UNIX required an intermediate level of computer power that was significant but attainable. A Silicon Graphics workstation with a 100-MHz IP22 processor and 64 Mbytes of RAM and a 1-GB hard disk was sufficient and used until 1994 to process images used in this work. A 3D image stack of a 510 × 310 pixel array and 20 optical planes could take up to 14 hr to deconvolve depending on the choice of α value and the number of iterations required for convergence. Smaller segments could be restored within 2–3 hr.

After 1994 the deconvolution algorithm was adapted to run on four 8-parallel processor boards (Scanalytics Division, CSP, Inc., Billerica, MA) decreasing the restoration time for a 510 × 310 × 20 image to 3 hr.

In June 1997, Signal Analytics Corporation Incorporated merged with Scanalytics, the biological imaging division of CSP, Inc. (Billerica, MA), to form a new

[54] E. D. W. Moore, E. F. Etter, K. D. Philipson, W. A. Carrington, K. E. Fogarty, L. M. Lifshitz, and F. S. Fay, *Nature* **365,** 657 (1993).

FIG. 6. A point source is deconvolved to a small volume compared to a transcription site that is deconvolved to a less dense and more asymmetric volume. Before deconvolution (A) and after deconvolution using a large α-value of 0.001 (B), point source (a 100-nm fluorescent latex bead, red arrow) and transcription sites (yellow arrows) appear very similar. (C–F) With decreasing α-values (0.0001, 1E-05, 5E-06, and 1E-06, respectively) the deconvolution brings the bead to a point source whereas the transcription sites comprise an irregular collection of voxels. The best solution is represented by (D) and (E). (D) and (E) converge to a minimum of residuals (Fig. 5) in a reasonable amount of processing time whereas longer processing with smaller α values does not appear to further improve the deconvolution.

corporation, Scanalytics Incorporated. Only a modified version of EPR, untested in this work, adapted to Microsoft Windows can be obtained from Scanalytics Inc., Fairfax, VA; info@scanalytics.com.

Relative Intensity Information Sufficient to Allow Accurate Image Processing but Not Interpretation

A fortuitous aspect of image formation theory is the abrogation of subjectivity. Relative intensity information, i.e., weighted point sources, is sufficient for accurate image processing and deconvolution. There is no need to interpret or make a value judgment about fluorescent sources, whether they represent a single point source or a superposition of multiple point sources.

Processing an image does not in itself provide any interpretation. The weighting factors provide relative intensity information, and after processing is completed, the interpretation of an image can only be in terms of relative intensities. This has been the major deficit and stumbling block for single molecule counting using fluorescence digital imaging.

Measurement of Intensity of One Fluorescent Probe to Provide Sufficient Information to Count Single Molecules Following Image Processing

What is the unit intensity of interest, that intensity or point source that represents a single fluorescent molecular probe? Image processing alone cannot a priori extract such information from a digital image. The a priori approach faces infinite possible solutions. An independent empirical measurement must be obtained to address this deficit. The unit intensity in question is not the same entity as the unit impulse $\delta(x, y)$. It is the unit point source intensity of the interrogation probe.

The availability of the cyanine dye series for labeling probes improved the signal-to-noise ratio of probes used for FISH due to the photo stability and large molar extinction coefficients of the dyes.[55] Fluorescein was also an acceptable dye because of its high quantum yield, although it was less photostable. Measurements indicated that interrogation probes could routinely be engineered to have total fluorescence intensities per probe that were greater than typical endogenous background signals in cultured cells. In such cases, the probe signal effectively became the primary contributor of fluorescence intensity to an image.

A conclusion, that will become more self-evident as data are examined, is that it is of utmost importance to know the unit intensity of one interrogation probe under imaging conditions. It is necessary in order to go beyond deconvolution and processing of images and progress to counting the number of fluorescent molecules. The goal to attain a more precise interpretation of the image data rests

[55] R. B. Mujumdar, L. A. Ernst, S. R. Mujumdar, and A. S. Waggoner, *Cytometry* **10,** 11 (1989).

with the ability to calibrate for the intensity expected of a single probe imaged through the optical setup.

Oligonucleotide Probes for Single Molecule Detection

Design of Fluorochrome-Labeled Oligonucleotide Probes

There are two major considerations in probe design to ensure the optimal interpretation of a fluorescence image. (1) To approach the theoretical potential to accurately describe the respective point source distribution in the true image, probes should be designed to conform as closely as possible to a point source. A single fluorochrome has limited spatial extent and therefore approaches a theoretical point source. Ideal probes would carry one fluorochrome. To realize adequate *S/N* three to five fluorochromes are more practical.[2] A DNA oligonucleotide probe with 50 bases has a linear extent of approximately 17 nm and therefore the attached fluorochromes approach the dimensions of a point source. (2) To ensure the accurate spatial localization of the probe relative to the target molecule, the fluorochrome must be tethered to the probe in a manner that maintains its spatial extent near to the probe and therefore also near to the target. Oligonucleotide probes hybridize within angstroms of their RNA or DNA targets. When they are conjugated to a fluorochrome via a relatively short linker arm, the fluorochrome is also constrained near the target (Fig. 1). The fluorescence emission of a hybridized probe then approximates a point source within angstroms of the target. Theoretically, maximum information can then be extracted about the spatial distribution of a probe and its respective target when the probe can be constrained close to the target and also treated as a fluorescent point source.

An appropriately designed probe will have four major attributes. (1) The probe is conjugated to fluorochromes that have adequate photostability to survive the continued exposure to excitation during optical sectioning. The presence of multiple fluorochrome molecules on one probe increases the probability that a target will continue to be detected through the entire stack of optical sections. The maximum intensity contributed by a probe is captured in the first optical section. Under our imaging conditions CY3-labeled probes faded at the rate of 2% per 2 sec exposure. After 20 optical sections the TFI of a CY3 probe would fade by approximately 40%. The probability that a probe will retain three out of five (60%) stable fluorochromes allows the continued detection of the target throughout the image stack. The total intensity contributed by CY3 probes to each optical section can then be corrected back to the total intensity of the first optical section to recover lost intensity information due to fading. (2) The probe has a defined size of 20 to 60 base pairs. The small size maximizes precision of hybridization to short sequences along the target nucleic acid. The probe may also consist of a collection of separate sequences iterated along a nucleic acid target, closely spaced,

to produce a point source with increased intensity. (3) Probes are engineered with a GC content of approximately 50% to effect efficient and specific hybridization of diverse sequences under the same hybridization conditions. (4) The probe has a constant TFI at a specific excitation/emission wavelength. The modified base, a thymine analogue with an amino linker arm, is spaced adequately throughout the probe sequence to prevent steric hindrance during labeling and also to prevent quenching of fluorescence once the fluorochromes are conjugated. The ability to define a constant TFI for a fluorescent probe allows accurate quantitation.

Such a probe will possess the appropriate attributes to be identified as a point source *in situ* and will provide accurate quantitative and spatial information about a molecular target in a single cell. Fluorochrome-labeled DNA oligonucleotide probes used in this work meet all the requirements for specific, quantitative molecular probes that emit fluorescence signal from spatial extents approaching that of a point source.[2]

Probes Optimized for Signal-to-Noise Ratio in Biological Samples

The major contributors to the decrease in *S/N* ratio within a hybridized sample can be divided into three categories: photoelectronic noise, electronic noise, and autofluorescence. Each category is described.

1. Photoelectronic (photonic) noise is inherent in the quantum nature of light and is modeled as random using a Poisson distribution.[56] The standard deviation is equal to the square root of the mean number of photons emitted. Therefore, a point source emitting an average of 475 photons per second results in a standard deviation of $\sqrt{475} = \pm 22$ photons of noise. The photon output of 10 fluorescence sources whose average photon output is 475 photons per second will show a statistical distribution curve (Fig. 7A).

2. Electronic noise contributes to the image after it is acquired. One example is CCD camera readout noise. Readout noise is random noise that is contributed once at the time of readout of the image. Older CCD cameras had higher readout noise. Readout noise was a major contributor to distortion of intensity information captured from low-light level fluorescence in the present work (Fig. 7B).

A typical *S/N* ratio for a scientific grade Photometrics Series 180 CCD camera similar to that used with our DIM is calculated using Eq. (8):

$$SNR = \frac{PQ_e t}{\sqrt{(P + B)Q_e t + Dt + N_r^2}} \tag{8}$$

substituting the following values for each parameter: P, photon flux incident on CCD, 475 (photons/pixel/second); B, background photon flux incident on CCD,

[56] K. R. Castleman, "Digital Image Processing," p. 414. Prentice-Hall, Upper Saddle River, NJ, 1996.

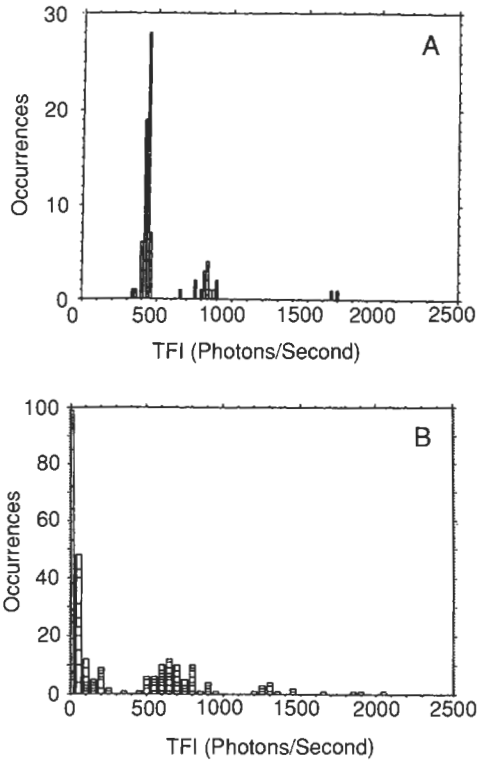

FIG. 7. The presence of random noise in an imaging system corrupts data. Histograms (A) and (B) show the theoretical extent of corruption of the TFI of point sources by random noise during the imaging process (contributed by Kevin E. Fogarty). A model, consisting of a collection of point sources of equal intensity scattered randomly onto a single plane that represents an array of pixels, was subjected to a convolution with an empirical PSF to simulate imaging through the optics of a light microscope. The intensity of the point source was chosen to be comparable to the intensity expected for one oligonucleotide probe labeled with five CY3 fluorochromes imaged through the DIM optical setup. (A) Photonic noise only. Photonic noise was added to 10 objects, each originally emitting 475 photons per second. The point sources were scattered randomly onto a single plane representing an array of pixels. The blurred image was deconvolved with the same empirical PSF from the DIM optical setup. Ten trials of 10 randomized objects were plotted as a histogram. The TFI of the restored objects was recovered as a distribution instead of a single value. (B) Photonic plus read noise. Photonic noise was added to 10 objects, each originally emitting 719 photons per second. The point sources were scattered randomly onto a single plane representing an array of pixels. The blurred image was then peppered with random noise as expected from the Photometrics Series 180 CCD camera readout. The new image was deconvolved with the same PSF as in (A). The deconvolved image was a Gaussian distribution of objects of varying intensity, with a mean close to the original intensity assigned to each point source. When the original signal was weak, i.e., from a single probe, the read noise had the greatest effect in corrupting an image signal.

0 (photons/pixel/second); Q_e, quantum efficiency of the CCD, 0.85; t, integration time, 2 (seconds); D, dark current, 1 (electrons/pixel/second); and N_r, read noise, 50 (electrons rms/pixel).

$$SNR = \frac{475 \times 0.85 \times 2}{\sqrt{(475 \times 0.85 \times 2) + (1 \times 2) + 50^2}} = 14$$

A graph of *S/N* vs. exposure time is plotted using this example (Fig. 8A).

The *S/N* ratio increases linearly with exposure time in the read-noise-limited region because an increase in exposure time accumulates more photons per pixel per unit time whereas the read noise, which is independent of time, remains the same. Therefore it is advantageous to increase exposure time when imaging low-level fluorescence in order to increase the *S/N* ratio. However, the stability of the fluorochrome must be evaluated and loss of signal due to fading must be weighed against increasing exposure time to provide an optimal increase in *S/N* ratio.

In the photon noise limited region there is less advantage to increasing the exposure time to improve the *S/N* ratio because the *S/N* ratio increases as the square root of the exposure time. Instead, acquisition of multiple shorter exposures may further improve the image through averaging of random noise.

As camera design improves, readout noise is decreasing. The Photometrics thermoelectrically cooled back-thinned CCD (model 180) camera used for this work had a readout noise of 50 electrons/pixel. Data acquired with the camera were read noise limited. A more recent Photometrics 200 Series CCD camera of comparable design had a readout noise of 12 electrons/pixel and comparable data acquired with the camera were photon noise limited (Fig. 8B). The lower read noise allowed an acceptable *S/N* ratio to be obtained using a 0.5 second exposure instead of a 2 second exposure.

Longer exposure times increase the number of photons emitted by a fluorochrome and therefore increase the *S/N* ratio. The brightest and most stable fluorochromes should be chosen in order to optimize the *S/N* ratio of probes against electronic noise. Especially where the target nucleic acid is known to occur in small copy number and/or single molecules, the fluorochromes of choice are CY3 and CY5, which emit in the red and far-red, respectively.

3. Autofluorescence is a major source of background inherent in biological samples that is contributed by biological components that have fluorescence absorption/emission in the same frequency range as the fluorescent probe of interest. The greatest amount of autofluorescence is exhibited in the blue and green emission spectrum of cells whereas the least is in the red through infrared. Autofluorescence is the major problematic factor remaining that dictates probe design. Longer exposure times cannot improve the *S/N* ratio of probe fluorescence versus autofluorescence. Using fluorochromes with high quantum efficiency and large extinction coefficients, linking multiple fluorochromes per probe (short probes, 24 to 60 nucleotides in length, can be linked with 3 to 6 fluorochromes, respectively, to

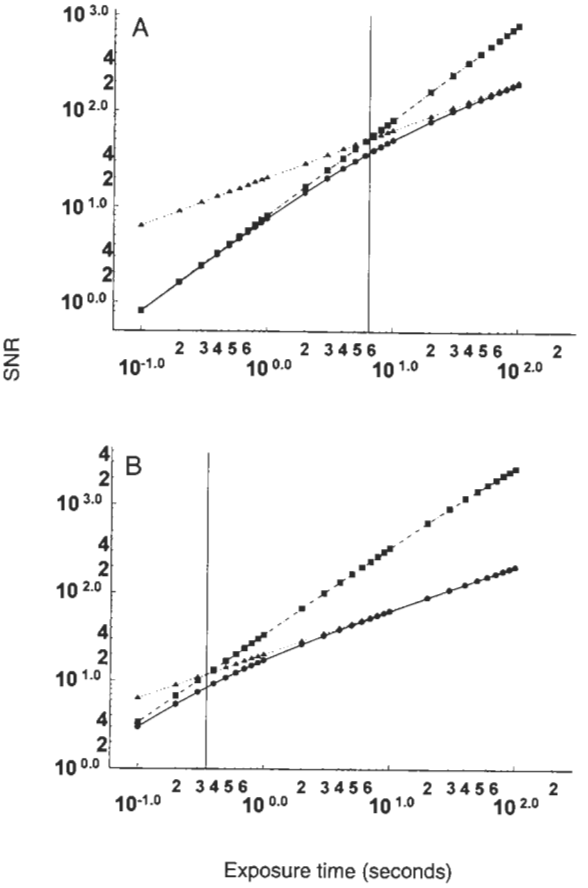

FIG. 8. Signal-to-noise ratios. Signal-to-noise ratios (*SNR*) are plotted as a function of exposure time (t) for two scientific grade CCD cameras using the equation $SNR = PQ_e t/\sqrt{(P+B)Q_e t + Dt + N_r^2}$. The plot area is divided into two regions at the intersection of the read-noise-limited equation $SNR = PQ_e t/N_r$ and the photon-noise-limited equation $SNR = PQ_e\sqrt{t}/\sqrt{(P+B)Q_e + D}$. The read-noise-limited region is designated to the left-hand side of the vertical line and the photon-noise-limited region to the right-hand side of vertical line. Photon noise ultimately limits the maximization of *S/N* as exposure time is increased (triangles). Read noise is the limiting factor for low-light level signal and short exposure time (squares). The camera read noise and the number of photons emitted per second from a source together determine the exposure time necessary to enter the photon-noise-limited region. (A) The Photometrics Series 180 CCD camera used in this work had the approximate *S/N* profile shown (circles) using read noise = 50 electrons rms/pixel and one fluorescent probe = 475 photons/pixel/sec. Any cytoplasmic signal originating from one fluorescent probe remained in the read-noise-limited region with exposure times of 2 to 3 sec per optical section. The respective signal-to-noise ratios were 14 and 20. (B) A Photometric Series 200 CCD camera had the approximate *S/N* profile shown (circles) using read noise = 12 electrons rms/pixel and one fluorescent probe = 475 photons/pixel/sec. The cytoplasmic signal for one fluorescent probe was in the photon-noise-limited region for exposure times of 1 to 2 sec per optical section. The respective signal-to-noise ratios were 17 and 26. The *S/N* was approximately two times higher compared to the Photometrics Series 180 CCD camera for the same exposure time. The advantage of lower read noise is reflected in the ability to use shorter exposure times that decrease fading while equal or better *S/N* is realized. The equations and plot format are taken from www.roperscientific.com.

ensure good *S/N* ratios), and iterating probes along the target sequence contribute the greatest advantage to improve the *S/N* ratio over autofluorescence. When a series of probes are iterated along a specific target sequence in such a manner that their closeness constitutes a fluorescence source that is small enough to be located in a single voxel, the signal emanating from that target will be amplified, increasing *S/N*. The total linear length of target should be restrained to about 140 nucleotides (48 nm of DNA at 3.4 Å/DNA base and 42 nm of RNA target at 3.0 Å/RNA base) or less in order to guarantee that the fluorescence source is as condensed as possible. Three 50-mer probes and up to five 25-mer probes could be iterated to a target and still remain a fluorescence source of approximately 50 nm in extended length.

Iteration of probes also helps to differentiate specific hybridization from nonspecific binding by their intensity differentials. There would be a decreased probability for random nonspecific targets to retain multiple probes compared to specific targets. Data will be presented in a later section that indicate nonspecific binding is negligible if appropriate conditions are used for FISH.

Some sources of autofluorescence can rival the intensity of the best probes. Efforts to discriminate autofluorescence from probe fluorescence through the use of spectral imaging is a potential solution to some of the current limitations of fluorescence imaging of single molecules at the higher emission frequencies. The emission spectra of a fluorochrome can be differentiated from the spectra of background autofluorescence and their respective contributions to pixel intensity can be calculated. An image representing only intensity information due to the fluorochrome can be generated.

A few practical measures that decrease autofluorescence include (1) the use of nutrient culture medium that does not contain phenol red, (2) fixation of samples with 4% *para*formaldehyde, and (3) using samples within 24 hr of fixation when the samples are stored in phosphate-buffered saline (PBS) at 4°.

DNA Oligonucleotide Probe Synthesis

The basic principles of synthesizing DNA generally, including oligonucleotide probes, are well known.[57] Those basic principles are applied to the design and synthesis of oligonucleotide probes used in this work.

A model 396 Applied Biosystems automated DNA synthesizer was used to synthesize probes used in this work. Typically, an oligonucleotide probe used in this work is obtained in a two-step process. The first step in the synthesis is to include a modified base at positions where a fluorochrome label is desired (Fig. 1). The preparation of amino-modified bases has been described in detail.[58,59] The

[57] M. H. Caruthers, *in* "Topics in Molecular and Structural Biology" (J. S. Cohen, ed.), p. 7. Macmillan Press, London, 1989.

[58] E. Jablonski, E. W. Moomaw, R. H. Tullis, and J. L. Ruth, *Nucleic Acids Res.* **14,** 6115 (1986).

[59] J. L. Ruth, *DNA* **3,** 123 (1984).

modified base used in this work is a thymine analogue that is available commercially as "Amino-Modifier C6 dT" (Glen Research, Sterling, VA), which is designed for use in conventional automated DNA synthesis. The synthesizer is run in the "Trityl On" mode to allow rapid purification of the modified oligonucleotide with an oligo purification cartridge (OPC). The second step is the covalent attachment of the fluorochrome label to each modified base. The purpose of the modified base used in the first step is to provide a functional group through which the fluorochrome label is covalently attached to the oligonucleotide in the second step. Various ligands can be conjugated to a DNA oligonucleotide probe through the amine derivatives.

The total number and spacing of the modified bases (and covalently attached fluorochrome labels) in the oligonucleotide can vary. Preferably, a modified base is incorporated within five bases from the 3′ end of the oligonucleotide and thereafter at approximately every tenth base position in the nucleotide sequence of the oligonucleotide. Incorporation of modified bases, and thus fluorochrome labels, closer than every 10 bases may cause quenching of fluorescence and concomitant loss of visual signal strength.

Fluorochrome Labels

Various fluorochromes are useful in labeling probes for adequate signal strength. Standard methods for attaching fluorochromes onto amino groups have been described.[60] Preferably the fluorochrome is CY3 or CY5 (Biological Detection Systems, Pittsburgh, PA), and also fluorescein (Molecular Probes, Inc., Eugene, OR). The advantages of CY3 include (1) high molar extinction coefficient for absorption of light at excitation wavelength, (2) high quantum efficiency of emission, (3) pH insensitivity, (4) good water solubility, and (5) a very strong peak in the Hg lamp (a popular excitation source) spectrum at the excitation frequency. Water solubility reduces nonspecific adsorption to membranes, which results in lower background. More recently Alexa dyes (Molecular Probes) for excitation by specific laser frequencies have comparable or better attributes for brightness and stability.

Conjugation of Cyanine Dyes to Oligonucleotides

Our experience has been that commercial fluorescent nucleotide labeling kits do not optimally label DNA with CY3 and CY5 (Amersham Pharmacia Biotech, Piscataway, NJ) when the standard protocols are followed.

Accepted Commercial Protocol. Dissolve 30 nmol of dry sample in 0.5 ml of 0.1 *M* carbonate buffer (pH 8.5–9.0) and add to the dye vial. Cap the vial and mix

[60] S. Agrawal, C. Christodoulou, and M. J. Gait, *Nucleic Acids Res.* **14,** 6227 (1986).

thoroughly. Incubate the reaction at room temperatue for 60 min with additional mixing at 15-min intervals.

This protocol was intended for a DNA oligonucleotide with one reactive primary amine.[61] The final reaction solution contains hydrolyzed dye molecules (free dye), oligonucleotides conjugated to one dye molecule, and unlabeled oligonucleotides. The oligonucleotides are separated from free dye with a Sephadex G-50 column. Labeled oligonucleotides are separated from unconjugated oligonucleotides using reversed-phase high-performance liquid chromatography (RP-HPLC).

The labeling efficiency of this protocol is about 20%. More efficient labeling required an alternative protocol.

Alternative Protocol. To effect overall labeling efficiency greater than 80% for modified DNA oligonucleotides with multiple alkyl amino group (1) the concentration of dye (FluoroLink, Amersham Pharmacia Biotech) is increased by decreasing the reaction volume from 500 μl to 30–60 μl, (2) the ratio of dye to amino groups is increased further by reacting less oligonucleotide, and (3) the oligonucleotide is carried through three consecutive labeling reactions.

Oligonucleotide A (MW 15,774): Stock = 1.65 μg/μl or 0.133 nmol/μl (five alkyl amino groups per oligonucleotide) and concentration of amino linker = 0.665 nmol/μl.

Use 7.5 μl of Stock oligonucleotide A (5.0 nmol of amino linker) and evaporate. Dissolve oligonucleotide A in 30 μl of 0.1 *M* carbonate buffer (pH 9.3) and pipette the solution into a vial of FluoroLink Cy3 monofunctional dye (Amersham Pharmacia Biotech). Cap the vial and mix thoroughly. Incubate the reaction at room temperature for 60 min with additional mixing at 15-min intervals. Let it stand for an additional hour. Transfer the reaction mixture to a new vial of FluoroLink Cy3. Cap the vial and mix thoroughly. Incubate the reaction at room temperature for 60 min with additional mixing at 15-min intervals. Let it stand for an additional hour. Add an additional 30 μl of 0.1 *M* carbonate buffer to the reaction mixture and transfer the reaction mixture to a third vial of FluoroLink Cy3. Incubate it as above.

Separation of Labeled Oligonucleotide from Free Dye

For quantitative work the probe preparation must be free of unconjugated dye. The presence of free dye will give an erroneous calibration of the TFI per probe. A rapid method for purification of labeled oligonucleotide from free dye can be accomplished with a Sephadex G-50 (Sigma, St. Louis, MO) column. Sephadex G-50 is placed in excess 10 m*M* triethylammonium bicarbonate (TEAB) and deaerated overnight. A column is built to a bed volume of 32 ml in a disposable serological 25-ml pipette plugged loosely with cootton at the tip, and washed with

[61] L. M. Smith, M. W. Hunkapiller, T. J. Hunkapiller, and L. E. Hood, *Nucleic Acids Res.* **13,** 2399 (1985).

gravity flow for 10 min using 10 m*M* TEAB. The reaction mixture is applied to the top of the column and eluted with 10 m*M* TEAB. Fluorochrome-labeled probe elutes first, separating away from the free dye. Collect 1.0-ml aliquots immediately into 1.5-ml microcentrifuge tubes following application of sample. A well-built column will separate the probe from free dye by at least 2 ml. Detect the fractions that contain fluorescent probe using ultraviolet (UV) illumination. Dry and combine the fractions. Repeat the separation if necessary using a fresh column. The purity can be checked using HPLC.

UV/VIS Absorption Spectrum to Determine Concentration and Labeling Efficiency of an Oligonucleotide Probe

The concentration of the labeled oligonucleotide stock solution must be determined accurately in order to prepare accurate dilutions of labeled probe that will be used to generate a calibration curve to determine the TFI of one probe under imaging conditions. A Beckman DU 640 UV/VIS spectrophotometer was used.

The concentration of any labeled oligonucleotide can be determined by the DNA absorbance at 260 using Beer's law: $A = \varepsilon cl$[A, absorbance; ε, extinction coefficient ($cm^{-1}\ M^{-1}$); c, concentration (M); l, 1-cm cuvette path length]. The extinction coefficient for a single-stranded oligonucleotide can be determined by summing the molar extinction coefficients for the individual bases multiplied by the number of each base A, C, G, and T (15,400A + 7,400C + 11,500G + 8,700T).

A more accurate method is to use a nearest neighbor calculation that includes nearest neighbor interactions of bases.[62]

$$2[\text{Sum}(E_{ab})] - [E2 + E3 + \cdots + E(n-2) + E(n-1)]$$

Where $\text{Sum}(E_{ab})$ is the sum of the pairwise extinction coefficients listed in the tabulation (http://www.genosys.com/technical) below and the E values are the normal single extinction coefficients for each individual base.

	3′Base			
5′ Base	A	C	G	T
A	13,700	10,600	12,500	11,400
C	10,600	7,300	9,000	7,600
G	12,600	8,800	10,800	10,000
T	11,700	8,100	9,500	8,400

Nearest neighbor calculations are given for ATGC and CGTA:

$$\varepsilon_{ATGC} = 2(11{,}400 + 9{,}500 + 8{,}800) - (8{,}700 + 11{,}500) = 39{,}200$$

$$\varepsilon_{CGTA} = 2(9{,}000 + 10{,}000 + 11{,}700) - (11{,}500 + 8{,}700) = 41{,}200$$

[62] C. R. Cantor and M. M. Warshaw, *Biopolymers* **9**, 1059 (1970).

The method of summation of molar extinction coefficients for individual bases does not differentiate between the sequences ATGC and CGTA:

$$\varepsilon_{ATGC} = \varepsilon_{CGTA} = (15{,}400^*1 + 7{,}400^*1 + 11{,}500^*1 + 8{,}700^*1) = 43{,}000$$

The fluorochrome labeling efficiency can be approximated by calculating the concentration of fluorochrome using the extinction coefficients (88,000 M^{-1} cm^{-1} at 490 nm, 150,000 M^{-1} cm^{-1} at 550 nm, 250,000 M^{-1} cm^{-1} at 649 nm) for fluorescein isothiocyanate (FITC) (pH 9.0), CY3 and CY5, respectively. An oligonucleotide with 5 amino linkers will be 80% or 100% labeled if the concentration of dye is four or five times that of the oligonucleotide, respectively. A precaution: to obtain valid information about labeling efficiency the probe must be pure with no free dye. Otherwise the DNA-to-dye ratio may erroneously show an apparently well-labeled probe.

Fluorescence *in Situ* Hybridization (FISH)

In situ hybridization with DNA oligonucleotide probes has evolved into a very straightforward process. Optimal hybridization conditions that provide high success rates have been published.[11,14] Most adjustments to the published techniques are a modification in the length of hybridization time and changes in concentration of formamide. Vanadyl adenosine complex and dextran sulfate were unnecessary components to obtain good hybridization results with DNA oligonucleotides.

The best results are obtained when care is taken to ensure similar melting temperatures, T_m, of all probes that are used for simultaneous hybridization. Oligo, Version 6.55 (Copyright 1989–2001, Wojciech Rychlik, Molecular Biology Insights, Inc.) software provides rapid assessment of T_m for any reasonable length sequence and GC content. This streamlines the choice of sequence and length of probe. In our laboratory sequences are chosen that have approximately 50% GC content. GC content has a dominant effect on T_m.

A typical hybridization protocol used in this work gives best results when cells are fixed for 10 min at room temperature in 4% *para*formaldehyde in phosphate-buffered saline (PBS) (2.7 m*M* KCl, 1.5 m*M* KH_2PO_4, 137 m*M* NaCl, 8 m*M* Na_2HPO_4). The cells are then washed and stored in PBS at 4° for less than 24 hr before hybridization.

Cells are gently permeabilized for 5 min in acetone at −20° and then placed in PBS moments before hybridization. Alternatively cells could be permeabilized using 0.5% Triton in PBS for 10 min and washed once with PBS before hybridization. A mixture of fluorochrome-labeled oligonucleotide probes, 50-mer, each at a concentration of 10 ng per probe per coverslip, is hybridized for 3.5 hr at 37° in 50% formamide containing 2× SSC, 0.2% bovine serum albumin (BSA), and 1 mg/ml each of *Escherichia coli* tRNA and salmon sperm DNA. Following hybridization, the coverslips are washed successively for 30 min in 50% formamide/2× SSC at 37°, 30 min in 50% formamide/1× SSC at 37°, and 3 × 15 min in 1× SSC at room temperature.

The coverslips are mounted on slides with antifade mounting media [100 mg phenylenediamine in 10 ml PBS (adjusted to pH 8.2–8.5 with 0.5 *M* $NaHCO_3$) and 90 ml glycerol]. Multicolored (green plus red, 0.099-μm-diameter, custom synthesis, or TetraSpeck 0.1 μm-diameter Molecular Probes) latex beads are included in the mounting media and used as fiduciary markers to align images from cells interrogated with dual-labeled (FITC and CY3) probes. The coverslips are sealed with clear nail polish and allowed to dry at room temperature in the dark. The hybridized specimens are now ready for quantitative imaging. Slides are stored in the dark at $-20°$ up to 1 year with no detectable deterioration.

Calibration of Fluorescence with Epifluorescence Microscope

Calibration Procedure to Measure TFI of One Probe under Imaging Conditions[1]

The TFI per probe molecule is measured by first imaging a series of calibrated solutions of the probe and plotting the number of probe molecules versus the measured fluorescence intensity to generate a regression curve. The TFI per probe is determined from the corresponding slope. To successfully calibrate the probe it must be purified from unconjugated dye molecules and the concentration of probe must be determined accurately.

First, an aliquot of the original fluorescent probe stock (0.1–2 μg/μl) used in an *in situ* hybridization is set aside for calibration. The absorption at 260 nm is measured with a UV/VIS spectrometer. The concentration of oligonucleotide probe is calculated using the extinction coefficient expected for the specific oligonucleotide sequence.

Second, a range of concentrations of fluorescent probe is prepared. All dilutions are prepared gravimetrically because the concentrations become too low for independent verification with a UV/VIS spectrometer. Aqueous dilutions (A) of approximately 10 and 20 ng/μl for Cy3-labeled probes, 130 ng/μl for FITC, and 15 and 75 ng/μl for Cy5 are prepared. Final dilutions (B) are prepared with 2.5-, 5.0-, or 10.0-μl aliquots of (A) plus phenylenediamine/glycerol mounting medium containing fluorescent beads that have fluorescence emissions different from the probe emission frequencies. The final solutions are adjusted to have the same percent water content. The final probe concentrations are chosen to be compatible with the exposure times and optical setup conditions used for imaging the respective hybridized specimens in order to make a useful calibration curve that is in the linear range of the CCD camera. Useful preparations for our optical setup contained final concentrations of probe between 0 and 4.0 ng/μl for CY3 probes, 0 and 30 ng/μl for FITC probes, and 0 and 8.0 ng/μl for CY5 probes. Five microliters of solution is placed between a coverslip and slide and sealed with clear nail polish. Exposure times of 2000, 3000, and 15,000 milliseconds were used to image CY3, FITC, and CY5, respectively.

A key step to calibrate the TFI per probe is to obtain an accurate measure of the number of probe molecules that contribute to the resulting TFI imaged at

a specific region of probe solution. The number of molecules imaged is in turn determined by the concentration of probe and the "imaged volume," which must be measured accurately. The imaged volume [imaged volume $= (x)(y)(z)\ \mu m^3$] is calculated using the effective pixel size at the specimen focal plane to calculate the area (x, y). The pixel size was calibrated for the optical setup of the microscope ($x = y = 93$ or 187 nm with a $\times 60$ magnification, 1.4 numerical aperature (*NA*) objective, and $\times 5$ or $\times 2.5$ camera eyepiece, respectively. The z dimension is measured as the distance between the inner surfaces of a coverslip and slide using fluorescent beads adhered to both surfaces to delimit the respective inner surfaces at the imaged region (Fig. 9). There is considerable variation in z between slides

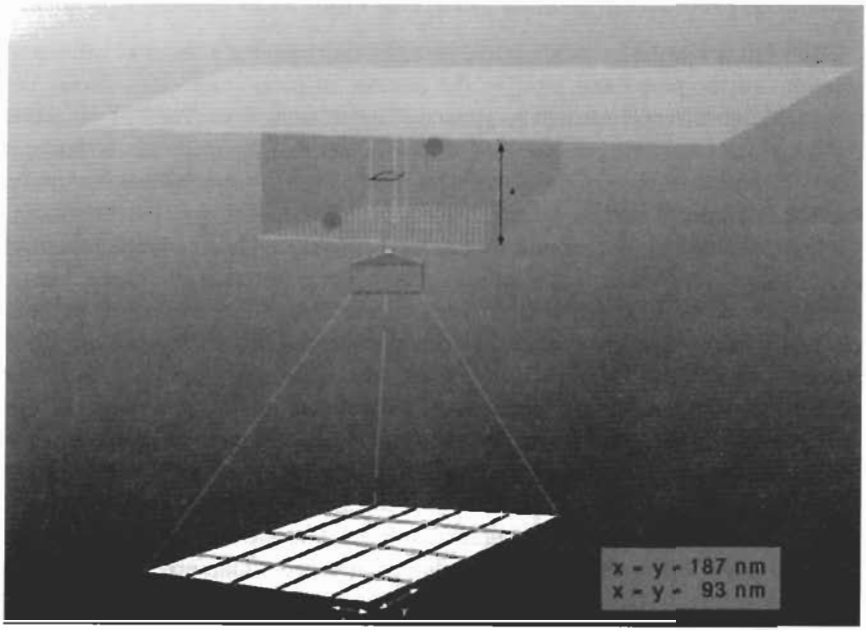

FIG. 9. Calibration of the TFI of one fluorescent probe molecule.[1] Each calibration solution, in succession, is placed between a coverslip and slide. Fluorescent beads (40–200 nm in diameter) adhere to the glass surfaces and delineate the distance between the inner surfaces of the coverslip and slide. The beads are brought into focus at each surface, while the stage position is monitored with an Eddy-current sensor, to measure the vertical distance (z) between the two beads. z is equal to the height of the volume element containing the imaged probe solution. The stage position was then set such that the focal plane was located equidistant from each bead. The dye solution was imaged at this focal plane. The image contained the total fluorescence contributed by all the fluorescent molecules in solution above and below the plane of focus in the imaged volume [imaged volume $= (x)(y)(z)$(number of pixels) μm^3]. The imaged volume included the full field of the CCD camera. The pixel size was calibrated for the optical setup of the microscope ($x = y = 0.093$ or 0.187 μm with a $\times 60$ magnification, 1.4 numerical aperture objective, and $\times 5$ or $\times 2.5$ camera eyepiece, respectively).

TABLE II
TFI CALIBRATION DATA FOR FITC-LABELED PROBE SOLUTIONS[a]

Sample (ng/μl)	File	Pixels	TFI	$z1$ (μm)	$z2$ (μm)	$z2 - z1$ (μm)
7.96	afsha	158100	532104736	−0.05	13.79	13.84
7.96	afsha′	75990	256890720	−0.05	13.79	13.84
7.96	afshb	158100	617296832	1.44	17.54	16.10
7.96	afshc	158100	585917696	2.06	17.66	15.60
7.96	afshe	144330	561355456	0.04	15.52	15.48
14.68	afsga	158100	943511936	0.55	13.50	12.95
14.68	afsgb	158100	895207872	0.45	11.98	11.53
14.68	afsgc	142800	848046528	0.32	12.19	11.87
26.85	afsfa	158100	1247529856	−0.05	8.92	8.97
26.85	afsfb	126990	963209280	0.65	9.01	8.36
26.85	afsfc	158100	1188750976	0.06	8.37	8.31
26.85	afsfe	158100	1328312960	−0.04	10.14	10.18

[a] Two slides were prepared for each dye concentration. Two to three widely separated locations were imaged on each slide. The number of sampled sites for a concentration of 7.96 ng/μl (column 1) was five. The image of a site consisted of one optical section located at position $(z2 - z1)/2$ on the z axis. The image consisted of a maximum of 510 × 310 array of pixels (column 3). One optical section contained the total fluorescence intensity, TFI (column 4), of all probe molecules above and below the plane of focus in the imaged volume. The imaged volume was equal to the area of the pixel array at the sample focal plane multiplied by the distance between coverslip and slide (187 nm × 187 nm or 93 nm × 93 nm per pixel) × (number of pixels) × $(z2 - z1)$ μm.

(5–20 μm) and also at different locations under the same coverslip. The number of probe molecules in the imaged volume is then calculated from the concentration of probe in the solution. One optical plane, midway between a coverslip and slide containing the fluorescent probe solution, is imaged. The TFI of the single plane represents signal emitted by all probe molecules in the volume above and below the imaged plane designated the imaged volume. A sample calculation of the number of probes imaged and the TFI per probe is provided below.

Sample data from one imaging session are tabulated in Tables II and III for FITC and used to generate the respective calibration curve. Table II contains measurements taken during microscopy. The probe concentration of the calibration sample is tabulated in the first column. The file name of the imaged plane and the total number of pixels in the imaged plane are in the second and third columns of Table II, respectively. The cumulative TFI of all the pixels in the imaged plane is shown in column 4 (Table II). The position of the bead on the inner surface of the coverslip ($z1$), the position of the bead on the inner surface of the slide ($z2$), and finally the difference $(z2 - z1)$ are tabulated in the fifth, sixth, and

TABLE III
SUMMARIZED CALCULATIONS FOR NUMBER OF FITC FLUOROCHROMES IN IMAGED VOLUME (nfiv)

Sample	imvol	Oligmol	nmiv	nfiv	tfipf
7.96 ng/μl					
Afsha	1.892491E−11	9.236778E−18	5562430	2.781215E+7	19.132097
Afsha′	9.096167E−12	4.439613E−18	2673555	1.336777E+7	19.217165
Afshb	2.201525E−11	1.074510E−17	6470746	3.235373E+7	19.079618
Afshc	2.133155E−11	1.041140E−17	6269791	3.134895E+7	18.690184
Afshe	1.932384E−11	9.431486E−18	5679684	2.839842E+7	19.767139
14.68 ng/μl					
Afsga	1.770792E−11	1.593088E−17	9593650	4.796825E+7	19.669510
Afsgb	1.576620E−11	1.418402E−17	8541682	4.270841E+7	20.960928
Afsgc	1.466036E−11	1.318916E−17	7942571	3.971286E+7	21.354458
26.85 ng/μl					
Afsfa	1.226564E−11	2.018533E−17	12155695	6.077847E+7	20.525850
Afsfb	9.182093E−12	1.511079E−17	9099789	4.549894E+7	21.169926
Afsfc	1.136315E−11	1.870012E−17	11261297	5.630648E+7	21.112150
Afsfe	1.392020E−11	2.290821E−17	13795426	6.897713E+7	19.257296

seventh columns (Table II), respectively. $(z2 - z1)$ is the height, z, of the imaged volume.

Calculation of Number of Probe Molecules in Imaged Volume

Data and calculations are presented for an FITC-labeled probe.

$c = 0.13008$ is the concentration of stock solution in grams/liter and molwt = 16,318 is the molecular weight of an unmodified DNA oligonucleotide comparable in sequence to the modified, fluorochrome-labeled probe. The molarity of the solution is the concentration (grams/liter) divided by the molecular weight:

$$M = c/\text{molwt} = \text{mol/liter}$$

$$M = 0.13008/16{,}318 = 7.9714\text{E–}06 \text{ mol/liter}$$

The area of one pixel of the CCD camera at the focal plane is determined by the optical setup and for $\times 60$ objective and $\times 5.0$ eyepiece is

$$\text{Pixel area} = 9.3\text{E–}08\,\hat{}\,2 \text{ m}^2$$

A representative measured z distance is 13.84 μm = 1.384E−05 m. (imvol) is the imaged volume in liters:

imvol = (z)(unit pixel area)(number of pixels)*1000

imvol = (1.384E–05)(9.3E–08 ^ 2)(158100)(1000) = 1.892491E–11 liters

Probe solution applied under a coverslip is a dilution of the stock solution:

$$\text{Aliquot of stock solution } (V_a) = 3.07\text{E}{-}06 \text{ liters}$$

$$\text{Final dilution volume } (V_f) = 5.0140\text{E}{-}05 \text{ liters}$$

$$\text{Final molar concentration } (C_f) = M^* V_a / V_f \text{ mol/liter}$$

$$(C_f) = (7.9714\text{E}{-}06)(3.07\text{E}{-}06)/(5.0140\text{E}{-}05) = 4.8808\text{E}{-}07 \text{ mol/liter}$$

(oligmol) is the moles of oligonucleotide in the imaged volume and (oligmol) is the product of the imaged volume (imvol) and the molar concentration of the probe solution:

$$\text{oligmol} = \text{imvol}^* C_f$$

$$\text{oligmol} = (1.892491\text{E}{-}11)(4.8808\text{E}{-}07) = 9.23687\text{E}{-}18 \text{ mol}$$

Avogadro's number = 6.022045E+23 (molecules/mole). The number of oligonucleotide molecules in the imaged volume (nmiv) is

$$\text{nmiv} = \text{oligmol}^* 6.022045\text{E}{+}23$$

$$\text{nmiv} = (9.23687\text{E}{-}18)(6.022045\text{E}{+}23) = 5.56248\text{E}{+}6 \text{ molecules}$$

A representative total fluorescence intensity of the imaged volume is

$$\text{tfi} = 5.321047\text{E}{+}08 \text{ arbitrary units}$$

The number of fluorochrome molecules in the imaged volume is

$$\text{nfiv} = 5^* \text{nmiv}$$

The total fluorescence intensity per fluorochrome is

$$\text{tfipf} = \text{tfi}/\text{nfiv}$$

A summary of pertinent calculated quantities for FITC probes is tabulated in Table III. The TFI values for varying concentrations of probe are obtained from the fourth column (Table II). The corresponding number of fluorochromes in the imaged volume (nfiv) are obtained from the fifth column (Table III).

The TFI is plotted against the number of fluorochromes to generate a regression curve to calculate the TFI of one fluorochrome under imaging conditions. The regression curves are generated using Mathcad 7 Professional. The y axis intercept indicates the level of background. Point determinations of TFI per fluorochrome (tfipf) are not accurate due to the presence of background that contributes a high percentage of TFI especially at low probe concentrations. On the other hand, the background does not affect the slope.

The slope and correlation coefficient R are summarized for CY3, FITC, and CY5-labeled probes (Fig. 10). The slope of the regression curve is equal to the

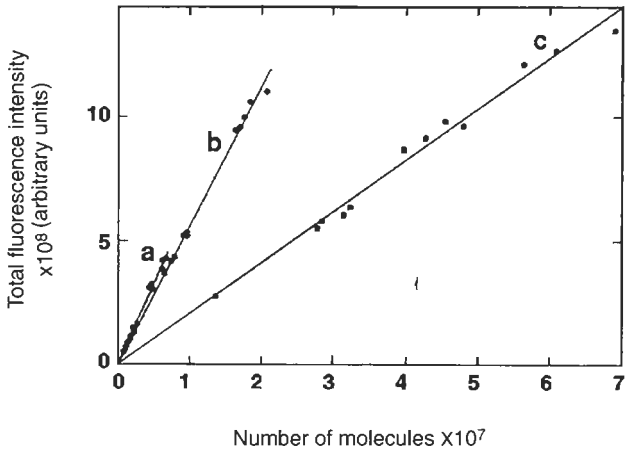

FIG. 10. The amount of light emitted per probe was calibrated by measuring the TFI from a known number of probes in an imaged volume. The TFI was plotted against the number of fluorochrome molecules (five per probe) to generate the regression curve. The slope is equal to the TFI per fluorochrome (curve a = CY3, $m = 65 \pm 1.3$, $R = 0.992$; curve b = CY5, $m = 56.3 \pm 1.4$, $R = 0.992$; curve c = FITC, slope $m = 20.6 \pm 0.8$, correlation coefficient $R = 0.985$). Exposure times for CY3, CY5, and FITC were 3, 15, and 4 sec, respectively. A normalized TFI per probe was used to calculate the number of probes hybridized at discrete point sources of light in a restored image. Reprinted with permission from A. M. Femino, F. S. Fay, K. Fogarty, and R. H. Singer, *Science* **280,** 585 (1998).

intensity per probe or per fluorochrome, depending on the plotted variables. In this instance, the slope indicates the TFI of one fluorochrome molecule. The intensity associated with one probe is equal to five times that value.

Imaging Hybridized Specimen and Acquiring PSF

Hybridized specimens, PSF beads (200 nm), and calibration solutions are all prepared with the same mounting medium and identical coverslips to minimize variation of refraction, reflection, and light scattering. The probes are calibrated after the hybridized specimens and PSFs are imaged but during the same session. The optical setup, which affects the PSF and the light intensity at the specimen, may change between imaging sessions.

The hybridized specimens are optically sectioned using 100-nm steps with 50 optical planes or 250-nm steps with 20 optical planes. The corresponding PSF is imaged with either 100 or 250-nm steps and at least twice the number of optical sections as the specimen.

TFI of One Probe Calculated from the Regression Curve Is Equal to the TFI of a Probe Imaged in One Plane

The collective intensity of pixels that comprise the Airy disk of a point source imaged in the focal plane is equal to this value. A single probe that is optically sectioned and then deconvolved to a point source has a different value of TFI.

Calculated TFI for One Probe Is Adjusted to That for an Optically Sectioned and Deconvolved Probe

Exhaustive photon reassignment (EPR), the deconvolution process used in this work, integrates light over a depth (number of optical sections) defined by the PSF. Therefore, the TFI of a single probe is adjusted to that for a deconvolved image by a multiplication factor equal to the number of optical sections in the PSF used for deconvolution of the specimen image. The number of optical sections in the PSF used in this example is equal to 50.

The TFI for one probe molecule is adjusted to that for a deconvolved image CY3 (65 TFI units/CY3 fluorochrome) $\times$ (5 fluorochromes) $\times$ (50 PSF z-planes) = 16,250 $\pm$ 975; FITC (20.5 TFI units/FITC fluorochrome) $\times$ (5 fluorochromes) $\times$ (50 PSF z-planes) = 5125 $\pm$ 600; and CY5 (56.3 TFI units/CY5 fluorochrome) $\times$ (5 fluorochromes) $\times$ (50 PSF z-planes) = 14,075 $\pm$ 1050).

The TFI of a single probe, adjusted to an appropriate value for a deconvolved image, is used to interrogate a deconvolved image of a fluorescence *in situ* hybridization specimen.

The Adjusted TFI of One Probe Predicts the TFI of Immobilized Probes on a Coverslip

To test the accuracy of the calibration procedure an independent measure of the TFI of one probe was obtained by imaging single immobilized probes.

Fluorescent probes are diluted to a concentration of 2–4 pg/μl in mounting media. Five microliters is placed between a slide and coverslip and sealed with clear nail polish. The sample is left in the dark at room temperature for 1 hr and then placed in the freezer for 24 hr to allow probes to adsorb to the surface of the coverslip. A majority of probes settle out onto the coverslip far enough apart to be resolved as individual probes. There can be an uneven distribution where some areas of the coverslip are devoid of probe.

The probes were not detectable when examining the microscopic field without the aid of a CCD camera. However, as the sample was optically sectioned and imaged, points of light came into view essentially in a single focal plane. The deconvolved image consisted of discrete objects having a range of intensities.

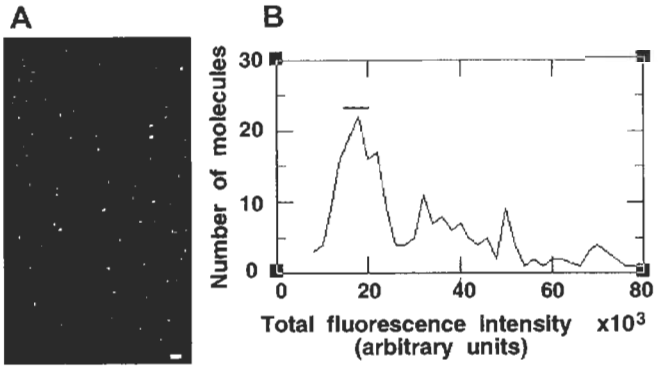

FIG. 11. Immobilized probes. (A) The accuracy of the calibration technique was tested by optically sectioning and restoring immobilized CY3-labeled probes adsorbed to glass coverslips. Pixel size = 93 nm. Bar: 1 μm. (B) Most frequent occurrences of TFI values per CY3 probe plotted as a histogram are comparable to the normalized value (solid bar) from the solution experiments. Reprinted with permission from A. M. Femino, F. S. Fay, K. Fogarty, and R. H. Singer, *Science* **280,** 585 (1998). Copyright © 1998 American Association for the Advancement of Science.

The mean TFI for an object was comparable to the calculated TFI for a deconvolved single probe (Fig. 11). The distribution of TFI of the immobilized probes mirrored the Gaussian TFI distribution of objects from the model system that included the random noise expected from the CCD camera used in these experiments (Fig. 7B).

Image Analysis

Interpretation of Digital Images

First, interrogation probes are small molecules. Small molecules provide an intrinsic level of precise spatial detail at molecular targets. The image, therefore, represents a collection of point sources of fluorescence that delineate the precise distribution and conformation of target molecules.

Second, the emitted light from point sources is detected on an array of pixels that has discrete boundaries. The pixels show a linear response to the intensity of light falling on the array. The intensity from one point source is distributed onto the pixel array according to the laws of diffraction.

Third, due to the Airy disk phenomenon, many pixels will detect some fraction of the light intensity from any single point source. Point sources, the basic unit in an image, appear as circular objects in the plane of focus due to the Airy disk pattern and as a cone in three dimensions. This is the PSF. A collection of spatially close point sources gives the appearance of a three-dimensional object due to the superposition of multiple, spatially distinct yet unresolved PSFs.

Fourth, an accurate model of the actual three-dimensional distribution of specific cellular molecules to which the fluorescent molecular probes have hybridized can in theory be reconstructed. Robust mathematical deconvolution algorithms applied to the fluorescence images can theoretically deconvolve the fluorescence information, using an empirical PSF, to estimate a true image.[63,64] The true image consists of point sources that are free of diffraction phenomena and other optical aberrations.

Fifth, the calibrated value for the TFI of one probe can potentially be used to identify sites in a restored image that represent one hybridized probe, the basic unit of fluorescence intensity in an FISH image. Therefore, interpretation of a fluorescent image should begin with the measurement of the TFI associated with objects in the deconvolved image.

Intensity Distributions in a FISH Image Are Hybridization Sites

It is important to establish statistical confidence in any new interpretation of FISH images and this is accomplished by analyzing the behavior of probes hybridized to specific targets. Analysis shows that probes bind to targets with predicted statistical probability, with predicted TFI, and with predicted spatial constraints.

First, the fluorescence intensity attributed to one fluorescent probe molecule is measured under imaging conditions.

Second, the amount of light emanating from a hybridization site is accurately measured. Optical sectioning and deconvolution are required. Optical sectioning provides complete spatial information necessary for successful deconvolution and reassignment of fluorescence signal to its point of origin in a 3D specimen. Reassignment of fluorescence signal to its point of origin facilitates the measurement of the total fluorescence intensity attributed to a hybridization site.

Third, the fluorescence intensity for one probe molecule, determined under imaging conditions, is corrected or normalized to be comparable to a hypothetical deconvolved single probe molecule. This allows a direct comparison of the intensity at a hybridization site in a deconvolved image with the predicted intensity of a probe molecule. Within statistical error the TFI representing a hybridization site occurs as multiples of the TFI attributed to one probe.

Fourth, to confirm a true hybridization site, three additional criteria are applied in addition to the TFI (Fig. 12). (1) The shape and (2) the size of a hybridization signal taken together establish the presence of a single hybridized probe, multiple probes, or noise. (3) Multispectral probes to a single target molecule must

[63] K. R. Castleman, *in* "Digital Image Processing" (A. V. Oppenheim, ed.), p. 293. Prentice-Hall, Englewood Cliffs, NJ, 1979.

[64] W. Carrington, *Proc. SPIE* **1205,** 72 (1990).

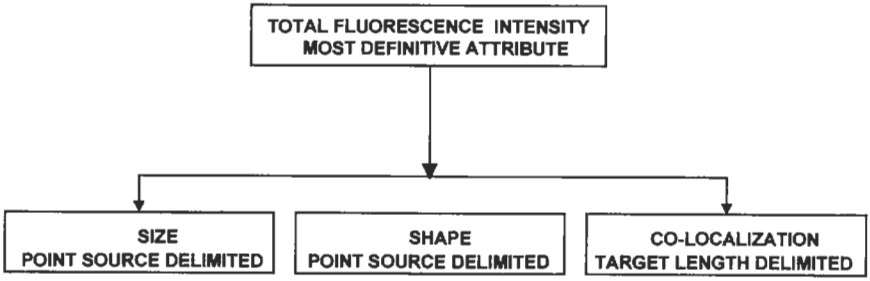

FIG. 12. The TFI is the most important criterion for identification of possible hybridization sites in a deconvolved image. A true hybridization site can be further confirmed through the requirement that the size and shape of the object conform to that expected for a deconvolved point source, especially if the TFI indicates the hybridization of a single probe (Fig. 17). More variable sizes and shapes are allowed when two or more probes are hybridized to different regions of a single target molecule, but are positioned close enough to remain unresolved. Two or more spectrally distinct probes hybridized to a single target molecule can further confirm a true hybridization site. The spatial constraints imposed by the selection and design of the probes will result in a predictable and distinctive colocalization pattern (Fig. 23).

show expected stoichiometry, colocalization, and predicted statistical probability distributions.

Fluorescence Signals Originating from Hybridization Sites Take on a Variety of Shapes and Sizes following Deconvolution

Deconvolution renders an image more amenable to quantitative analysis. Deconvolution aids the quantitative interpretation of hybridization sites in an image by placing the entire signal associated with a point source into a small concentrated volume in three-dimensional space. The deconvolution process also results in an increase in the definition of the boundaries of an isolated point source.

The history of the specimen to be analyzed is described briefly. Serum-starved, cultured normal rat kidney (NRK) cells were induced with serum, fixed, and hybridized with five probes targeted to the 3′-UTR of β-actin mRNA. The probes consisted of five different sequences, 50 nucleotides in length, each labeled with five CY3 fluorochromes. The five probes were iterated in close proximity to each other on the nucleic acid target (Fig. 13). The specimen was imaged with optical sectioning. A PSF was acquired. The probes were calibrated during the imaging session. The image stack was deconvolved using EPR with 400 iterations and an alpha value of 5×10^{-6}. The deconvolution converged minimizing the residuals to 10%.

A point source or single probe deconvolves to a 3D cluster of contiguous voxels and therefore the TFI of one probe is fractionally distributed among those voxels.

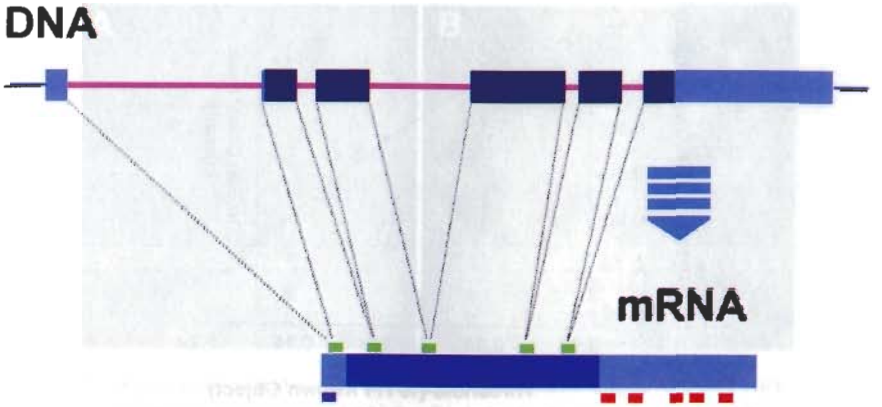

FIG. 13. A schematic depicts the rat β-actin gene and a typical processed β-actin messenger RNA. The positions of some representative oligonucleotide probes used in this work are shown hybridized to their target sequences (3′-UTR probes, red; splice junction probes, green; and one 5′-UTR probe, blue). The sequence of the β-actin gene is that published by U. Nudel, R. Zakut, M. Shani, S. Neuman, Z. Levy, and D. Yaffe, *Nucleic Acids Res.* **11,** 1759 (1983) (accession J00691). The nucleotide sequence for DNA is color coded for the 5′- and 3′-UTR (light blue), introns (pink), and exons (dark blue). The RNA nucleotide sequence is color coded for an open reading frame in the processed messenger RNA (blue) and the 5′- and 3′-UTR (light blue).

A deconvolved image also has many low intensity voxels that represent autofluorescence or background signal. A cell brought through a mock hybridization provides a representative intensity distribution of the autofluorescence and background signal. An appropriate threshold is applied to the images. All pixels with values less than the threshold value are set to zero generating a modified image. The threshold value should be low enough to minimize the loss of lower intensity voxels from the cluster that represents a single hybridized probe, but high enough to remove greater than 90% of the voxels attributed to autofluorescence signal within cells. The threshold was chosen to be less than 10% of the TFI expected for a single probe labeled with CY3. Setting a threshold facilitated the automated analysis of objects in the cell by creating discrete objects. A model, generated using the average value of the TFI of a single CY3 probe, was used to verify the process to establish a threshold, and showed that the criteria were valid for preserving the TFI of one probe (Fig. 14).

A binary mask was placed on the deconvolved image to exclude signal outside the boundary of the cell that was chosen for analysis. This was accomplished using an interactive computer program to trace along the outer edges of the cell membrane in each plane of the deconvolved image. There was enough autofluorescence to determine the cell boundary using the FITC image. The collection of boundary outlines from all the optical planes was then interpolated through the z axis to

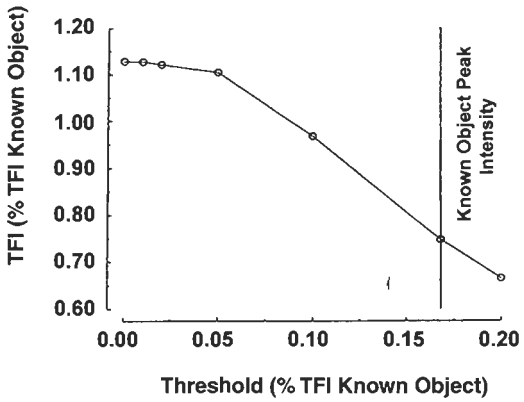

FIG. 14. A conservative calculated threshold minimized the adverse effects of background and noise on the measurement of the TFI of an object. Further analysis of the model system (Fig. 7B) indicated that setting a threshold at 10% of the total expected intensity of a single probe minimized the error for measuring the TFI of objects that represent single probes amid background noise (contributed by Kevin E. Fogarty). The average peak pixel intensity (maxima) within an object representing one probe falls at 17% of the TFI. This theoretical analysis supported the methodology that had been implemented for single molecule detection. A threshold that was too low did not separate objects adequately from background pixels and resulted in larger objects with TFI greater than 100% of that expected. A threshold that was too high removed pixels that were an integral part of the object leaving only the most intense pixels, those close to the object's peak intensity or maxima. Empirical data from immobilized fluorescent probes (Fig. 11) indicated that setting a threshold between 4.5 and 10% of the expected TFI minimizes the perturbation of the TFI of imaged objects. The data were for probes labeled with five CY3 fluorochromes and imaged with the described DIM system.

produce a shell delineating the volume of a single cell. The mask, when superimposed on the entire image, set to zero the value of all pixels outside of the shell boundary while leaving all pixel values inside the shell volume unchanged. This process facilitated an automated analysis of a specific region of interest (ROI) by segregating out the unwanted information, in this case every signal outside the perimeter of one cell. The remaining signal is a collection of discrete objects (Fig. 15A).

The experiment required two controls. The first control sample was hybridized with CY3-labeled probes specific to the 3′-UTR of α-actin mRNA. α-Actin is an isoform of actin found in muscle cells but not expressed in NRK cells. Such a control provided information on nonspecific binding of probes and was an indicator of good hybridization conditions. Optimal hybridization conditions provide adequate stringency for specific binding of β-actin probes and concomitantly reduce nonspecific binding to essentially zero (Fig. 15B). The second control cell was brought through a mock hybridization in which the labeled probes were omitted. The control provided information concerning the distribution profile of intensities

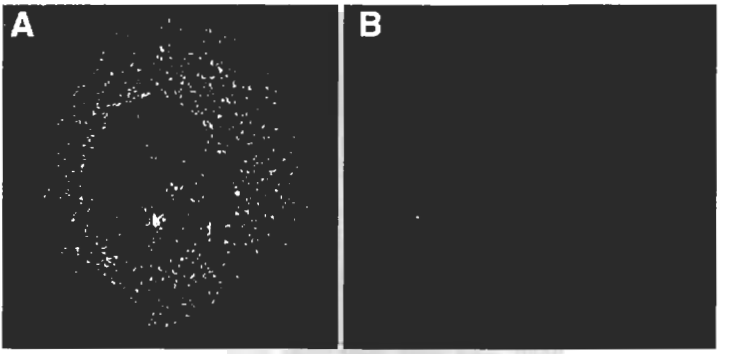

FIG. 15. Oligonucleotide probes only hybridize to their specific targets. Cultured NRK cells are induced for 15 min with serum and fixed. (A) A cell is hybridized with CY3-labeled probes targeted to the 3′-UTR of β-actin mRNA; 513 objects are detected, each having a TFI equaling one to five probes. Two transcription sites are also visible. (B) A cell is hybridized with CY3-labeled probes targeted to the 3′-UTR of α-actin mRNA; 20 objects are detected, each having a TFI equal to one probe hybridized. The α-actin gene is not induced by serum in NRK cells. The number of objects is equal to that found in a mock hybridization, and therefore can be considered background. The conclusion is that using carefully selected and controlled hybridization conditions, oligonucleotide probes do not contribute to background through nonspecific binding.

associated with autofluorescence. The control cells were deconvolved, processed, and analyzed with the exact steps used for the experimental cells.

The mock hybridization was analyzed to characterize the remaining autofluorescence contribution to a fluorescence image after applying a threshold (Fig. 16A). Autofluorescence originates from point sources that represent uncharacterized cellular components and has variable intensities. Analysis of an image hybridized with fluorescent probes to target sequences contains, in addition to the specific signal, a distribution of objects above threshold similar to that seen in the mock hybridization (Fig. 16B).

Predicted Shape and Size of Deconvolved Point Source

The discrete nature of the pixel array in the detector causes the raw signal to be detected as spatially discontinuous units of intensity rather than continuous variations of intensity. The perfect deconvolution would in principle place every point source at its respective spatial location. Ideally, one would expect the location to be in a single voxel. In practice this does not happen.

Through the use of the quantitative method described here that identifies true point sources by their TFI, empirical evidence indicates that a deconvolved point source that represents a single hybridized probe is present as a collection of contiguous voxels in 3D space. The exact number of contiguous voxels and their distribution in 3D space are dependent on several factors. The position of the point

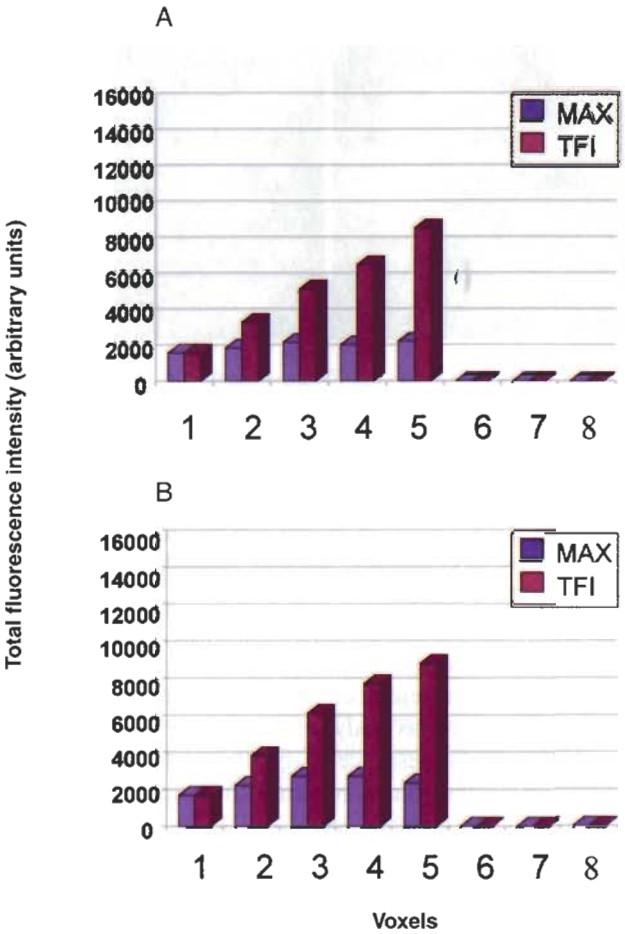

FIG. 16. Objects that have a TFI less than the TFI of one probe range in size from one to five voxels. The objects are considered background. The voxel with the maximum intensity in each object is not markedly higher than other voxels in the object. The increase in the TFI of objects is directly proportional to the increase in the size of the objects. (A) In a mock hybridization, the background objects are the major source of fluorescence. (B) In a cell hybridized with CY3-labeled probes to the 3′-UTR of β-actin, the background objects have a profile indistinguishable from the mock hybridization.

source in the specimen relative to the discrete pixel boundaries on the detector and the position relative to the focal plane in the series of optical sections will affect the shape of the cluster (Fig. 17). The sampling rate will additionally contribute to the size or number of voxels that makes up the object. Over sampling, using a voxel size smaller than the resolution limit will increase the size of a restored object.

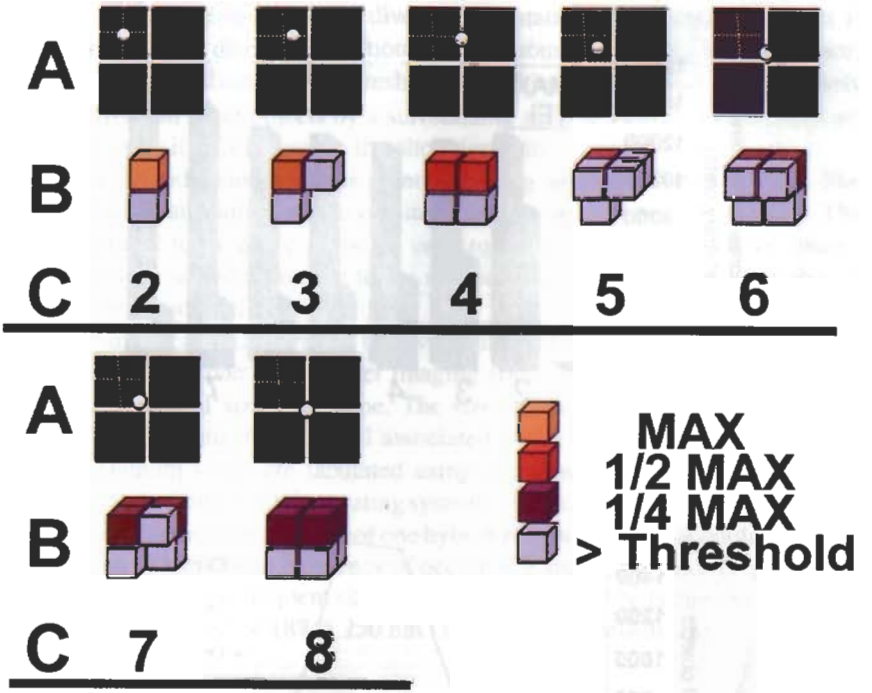

FIG. 17. The discrete nature of the pixel array detector and the discontinuous stepping associated with optical sectioning precludes the deconvolution of a point source to a single voxel, except in the one instance where the point source is exactly centered in a pixel and is in the focal plane. (A) A group of four pixels is shown. A point source is located at possible positions in one pixel. When the point source lies on an edge or at a vertex it, shares its TFI equally with two or four adjacent pixels. (B) The TFI of a point source imaged in the focal plane will be deconvolved to one maximal voxel (yellow) if it is centered in a pixel. If the point source is centered but out of the focal plane it will share a fraction of the TFI with an additional voxel along the optical axis (light blue). The TFI will be equally shared by two voxels (dark orange) if the point source is in the focal plane but located at an edge and four voxels (maroon) if it is in the focal plane and located at the vertex of four pixels. If the respective point sources are not exactly in the focal plane, their TFI will be shared with additional voxels along the optical axis (light blue) resulting in objects of four and eight voxels, respectively. Voxels that share a fraction of the TFI that falls below threshold are not shown and give the appearance of asymmetry to some objects. (C) The total number of voxels that can represent a deconvolved point source, theoretically, can range from one to eight as shown by this model. Empirical data acquired using probes that approach a theoretical point source support this model (Figs. 18 and 23).

Criteria to Identify Hybridization Sites to 3′-UTR of β-Actin mRNA in Deconvolved Image

A single CY3-labeled probe molecule, under imaging conditions, has the measured value, in this particular example, of 12,000 TFI units. Examination of the processed fluorescence image reveals objects varying in size and shape that conform to the expected TFI of one to five probes.

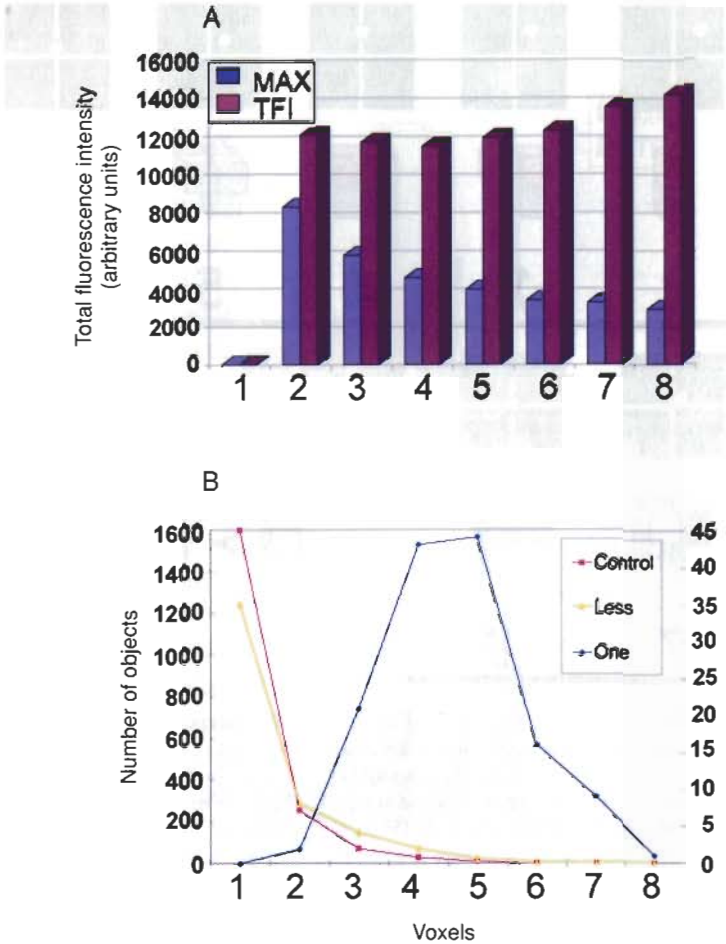

FIG. 18. Objects that represent one hybridized probe are characterized. An NRK cell, hybridized with CY3-labeled probes targeted to the 3′-UTR of β-actin mRNA, is imaged and deconvolved. Objects in the deconvolved image whose TFI falls in the range of one probe hybridized (12,000–14,000 arbitrary units) are selected for further analysis. Their maximum pixel intensity, size (number of contiguous voxels), and frequency of occurrence are plotted. (A) Clusters ranging in size from two to eight contiguous voxels have a TFI expected of one hybridized probe. The maximum intensity voxel has the highest values in the smaller objects and the lowest values in the larger objects. This conforms to the subpixel placement of point sources (Fig. 17). (B) The most frequent sizes associated with objects representing one probe are three to six voxels, with four and five the most probable. Subpixel placement of point sources predicts that the least probable sites are those with the least redundancy such as the center of a pixel or the vertex formed by four pixels. The least probable sites result in one, two, or eight voxel objects. "Control" represents the objects in a mock hybridization (left ordinate). "Less" represents objects in a hybridized cell that have a TFI less than that expected for a single probe (left-hand ordinate). "One" is a histogram of the objects that represents one probe hybridized (right-hand ordinate).

How should we interpret the diverse presentation of objects? An object is herein defined as a discrete collection of contiguous voxels (i.e., sharing a face) remaining after application of a threshold. The object, in 3D space, is completely separate from all other objects by a surrounding shell of voxels that has been set to zero because it falls below the threshold intensity.

A true hybridization site was identified using several different criteria. The most definitive attribute, and the one used initially in this study, is the TFI. The TFI, calibrated for a single probe, is used to analyze the objects in the image. The objects are sorted according to the number of probes hybridized (number of probes hybridized = TFI/(TFI/probe).

Once an object is determined to have an intensity that is at least equal to the measured value of one probe under imaging conditions, it is further scrutinized for the attributes of size and shape. The size (number of voxels), TFI of each object, TFI of the maximum voxel associated with each object, and coordinates of the maximum voxel are tabulated using a computer program ("countobjs," Lawrence M. Lifshitz, UNIX operating system). A histogram shows all objects with a TFI value near the expected TFI of one hybridized probe sorted according to size, on the x axis. The TFI and frequency of occurrence are on the y axis (Fig. 18A, B) respectively. The most frequent size for one hybridized probe is three to six voxels for a voxel size of 187 × 187 × 250 nm (x, y, z) after thresholding.

Quantitative Analysis of Hybridization Sites to Identify Single Molecules of β-Actin mRNA

Many hybridization sites are identified that have hybridized a single probe. Other sites show hybridization of multiple probe molecules (Table IV and Fig. 19). The original hypothesis was that a true hybridization site would be unequivocally identified through the use of iterated probes that hybridize to multiple sites along the 3′-UTR sequence, but that a single probe hybridized at a site would be indistinguishable from probes adhering nonspecifically to cellular components. However, it appears that there are many sites that hybridize a single probe. These sites cannot be discounted as nonspecific binding because the control cell that is hybridized with probes specific to α-actin mRNA shows very low numbers of objects that are identified as single hybridized probes similar to a mock hybridization (Fig. 15B, Table V, Fig. 20). Because the amount of nonspecific binding in a control probe is at best minimal, the interpretation is that greater than 90% of single probe sites represent a true target. The quantitation process combined with deconvolution facilitates a more accurate interpretation of fluorescence images. The conclusion is that quantitative analysis of hybridization sites identifies single molecules of β-actin mRNA.

Important information about the success of the deconvolution process emerges from the identification of single hybridized probe molecules in a 3D image. The

TABLE IV
FLUORESCENCE *in Situ* HYBRIDIZATION TO THE 3′-UTR OF β-ACTIN mRNA[a]

Number of probes hybridized	A (100% CY3)		B (100% CY3)	
	Number of objects	Percent of total	Number of objects	Percent of total
1	184	35.9	123	43.5
2	154	30.0	88	31.1
3	84	16.4	47	16.6
4	49	9.6	18	6.4
5	42	8.2	7	2.5
>5	10	—	18	—
Total objects (1–5 probes)	513	100.0	283	100.0

[a] Cells were hybridized with five different CY3-labeled probes and show objects hybridizing one to five probes. Objects from two cells (A and B) are sorted according to intensity. The objects are tabulated according to the number of probes hybridized.

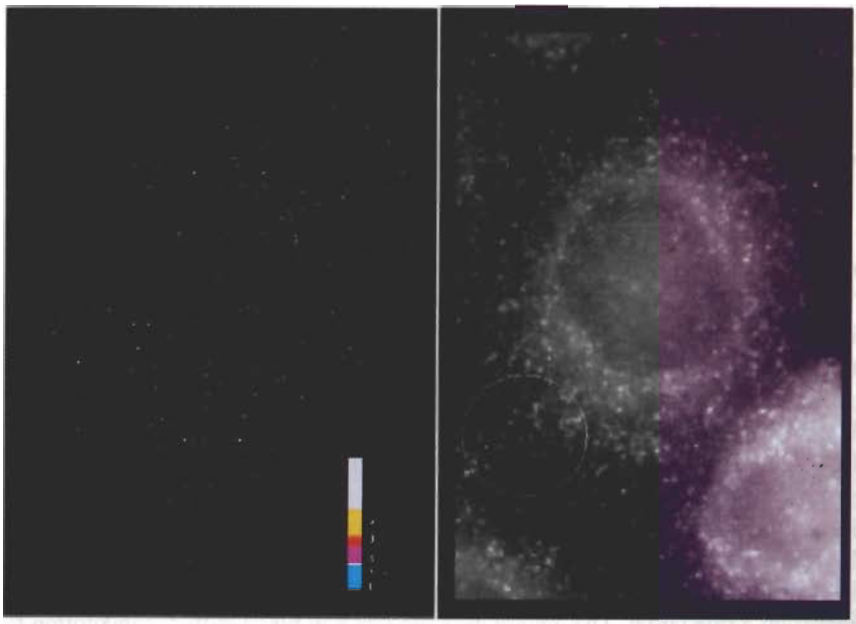

FIG. 19. Single molecules of β-actin mRNA are detected *in situ*.[1] (Right panel) A serum-starved NRK cell is hybridized with CY3-labeled probes to the 3′-UTR of β-actin mRNA and imaged. (Left panel) The TFI of each object in the deconvolved image is mapped to a single voxel at the coordinates of the respective maximum voxel. The single voxel objects are then color coded according to the number of probes hybridized. Most objects represent one to five probes hybridized, the number expected to hybridize a single β-actin mRNA. [1 = green, 2 = blue, 3 = pink, 4 = red, 5 = yellow, and >5 = white.]

TABLE V
CONTROLS IN HYBRIDIZATION[a]

	Mock hybridization (CY3)		α-Actin (CY3)	
Number of probes	Number of objects	Percent of total	Number of objects	Percent of total
1	22	73.3	20	100
2	6	20.0	0	0
3	2	6.7	0	0
4	0	0	0	0
5	0	0	0	0
>5	7	—	0	—
Total objects (1–5 probes)	30	100.0	20	100.0

[a] A mock hybridization and hybridization to α-actin, an mRNA not expressed in NRK cells, show about 20 objects that have the intensity of one hybridized probe.

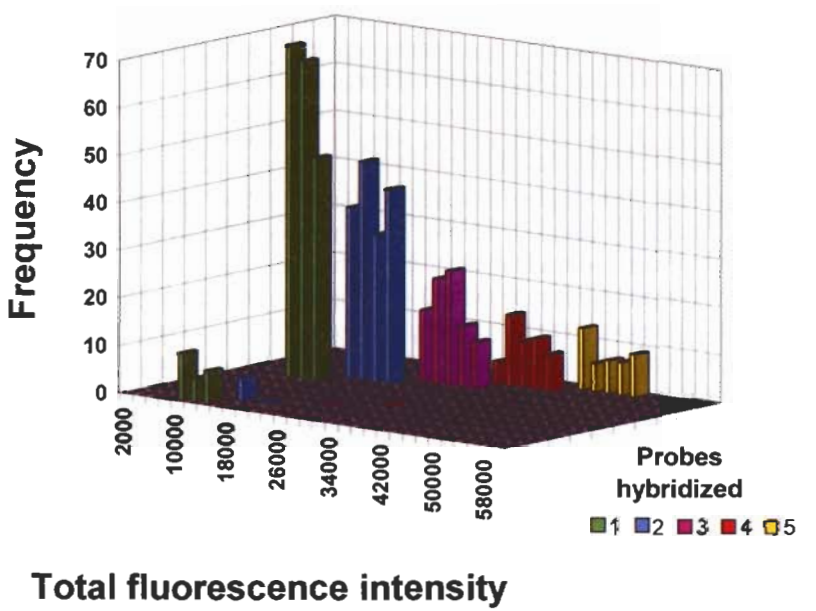

FIG. 20. A histogram shows the frequency of objects detected in a cell according to their TFI. Each range of TFI is color coded for the number of probes hybridized. The front row represents objects in a cell carried through a mock hybridization. The second row represents objects in the cell depicted in Fig. 15A. The most frequent occurrences are objects representing one and two probes hybridized. Sites hybridizing three to five probes are less frequent.

observation that the TFI of a deconvolved point source is not contained in a single voxel, but is instead distributed in a contiguous cluster of voxels, in retrospect, seems appropriate (Fig. 17). The cluster of voxels, taken together and summed, contains the expected intensity of one hybridized probe and also has a finite volume. This observation has many consequences, as will be seen in the ensuing pages. This is the first time a fluorescent "object" has been interpreted *de novo in situ*.

The analysis of single probe hybridization sites indicates that the most common dimensions for a single probe acting as a point source is usually two to seven voxels after deconvolution and thresholding for a pixel size of 187 × 187 × 250 nm. According to the model depicted in Fig. 17 the object size increases systematically as the point source location approaches an edge or a vertex of a pixel away from the center of a pixel. Therefore, the size of objects representing single probes in an image may reflect the subpixel position of the point source.[65]

The size, shape, and TFI of an object in the deconvolved image may also contain some contribution from random noise. The lowest intensity signals, such as those representing single probe hybridization sites, will be most affected by corruption due to random noise. The effect of random noise is to widen the range of values attributed to the TFI as well as to influence the shape and size of the deconvolved objects (Fig. 7B). The largest contributor to random noise in low-level fluorescence is readout noise from the CCD camera electronics (Fig. 8A).

Hybridization Behavior as Predicted by Statistics

Data indicate that single molecules of β-actin mRNA are detected. Can the results be rigorously tested or verified? One method is to hybridize competing probes labeled with spectrally distinct fluorochromes.

A set of five probes specific to the 3′-UTR of β-actin is conjugated to CY3 and also to FITC. The two sets are then combined as a 50 : 50 mixture. Serum-starved NRK cells are induced with serum and fixed at 15 min. The cells are hybridized with the 50 : 50 mixture of CY3 and FITC-labeled probes. Other samples are separately hybridized with a set of 100% CY3-labeled probe or 100% FITC-labeled probe. The probes used for hybridization are calibrated for the optical setup. The samples are optically sectioned and deconvolved using 400 iterations and an α-value of 5×10^{-6}.

The objects in the deconvolved images are analyzed and categorized according to the number of probes hybridized. The objects detected in the CY3 channel from a cell hybridized with the 50 : 50 mixture are compared to a distribution of

[65] W. A. Carrington, R. M. Lynch, E. D. W. Moore, G. Isenberg, K. E. Fogarty, and F. S. Fay, *Science* **268,** 1483 (1995).

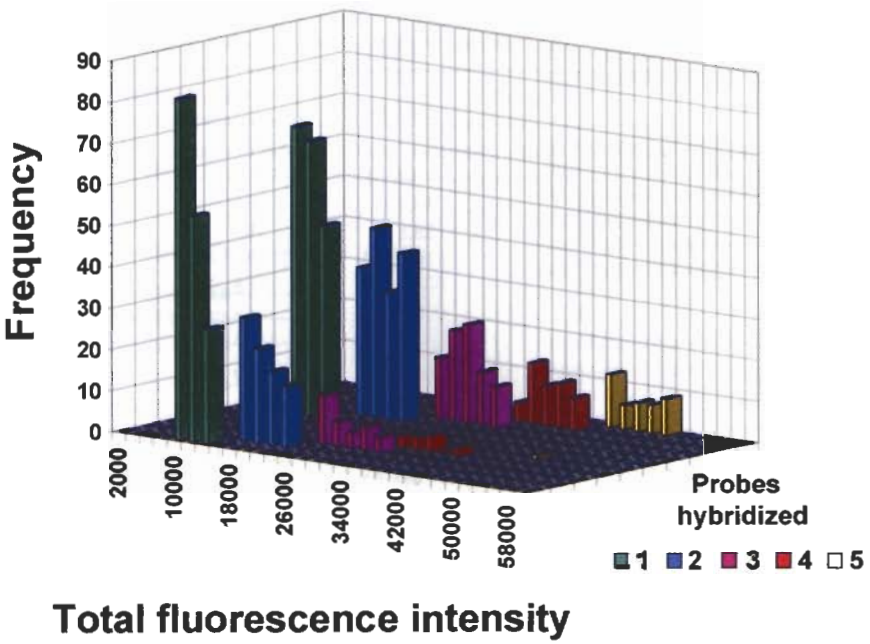

FIG. 21. A histogram shows the frequency of objects detected in a cell according to their TFI. Each range of TFI is color coded for the number of probes hybridized. The front row represents CY3-labeled objects in a cell hybridized with a 50:50 mixture of CY3 and FITC-labeled probes to the 3′-UTR of β-actin mRNA. The back row represents a cell hybridized with 100% CY3-labeled probes. (Front) The CY3- and FITC-labeled probes compete with each other. The relative number of objects hybridizing one CY3-labeled probe increases above that found in the cell hybridized exclusively with CY3-labeled probes, while the number of objects hybridizing three, four, and five probes decreases dramatically.

objects from a cell hybridized with 100% CY3 label (Fig. 21). The CY3 signal becomes diminished in the cell hybridized with the 50:50 mixture of probes. This is expected when the hybridization is specific, because some of the specific binding due to the CY3 probe will be competed by the FITC probe. If the hybridization sites are in fact just nonspecific sticking, the signal could become additive with the result that the CY3 probe signal would remain largely unchanged.

There is a decline in the number of objects hybridizing three, four, and five probes, but surprisingly, an increase in the number of objects hybridizing one CY3 probe. The total number of objects can vary between cells. Therefore a better indication of a change between the 50:50 mixture and the 100% CY3 hybridization is a look at the relative distribution of objects within a single cell. The fraction of objects in a single cell that represents one hybridized CY3 probe

TABLE VI
A COMPETED HYBRIDIZATION

	afsc2 (CY3)		afsd1 (CY3)	
Number of probes	Number of objects	Percent of total	Number of objects	Percent of total
1	166	55.7	201	57.6
2	86	28.8	108	30.9
3	32	10.7	30	8.6
4	13	4.4	8	2.3
5	1	0.3	2	0.6
>5	16	—	5	—
Total objects (1–5 probes)	298	100.0	349	100.0

molecule increases from a range of 36–43% in a cell hybridized with 100% CY3 probes (Table IV) to approximately 56% in the competed hybridization (Table VI).

How can this be explained? The answer lies in the statistical probability distribution of hybridization to the 3′-UTR when the access to some target sequences is limited. The profile of hybridization to the 3′-UTR of β-actin mRNA indicates that one or two hybridization sites on a single mRNA molecule is the most frequent occurrence (Fig. 19 and Fig. 20). Target sites are not equally accessible at all times due to possible secondary structure or bound proteins.[66] A diagram depicts probable hybridization patterns that occur for a 50 : 50 mixture of CY3 and FITC probes targeted to the 3′-UTR of β-actin mRNA (Fig. 22). The diagram clarifies the phenomenon of an increase in the number of objects that has hybridized one probe when hybridization is carried out with a 50 : 50 mixture of CY3- and FITC-labeled probes.

The diagram illustrates how sites that normally hybridize one probe will be hybridized with either a CY3 or FITC probe (Fig. 22A). Therefore, the number of objects hybridizing one CY3 probe should decrease by 50%. The empirical data show an increase in the relative number of objects that hybridize one CY3 probe (Fig. 21 and Table VI). The mRNA molecules that hybridize two probes have a 50% probability of hybridizing one CY3 and one FITC probe simultaneously, due to redundant permutations, but only a 25% chance of hybridizing two CY3 probes. Therefore the number of objects hybridized to two CY3 probes would be diminished by 75% of that expected from hybridization using 100% CY3 probes. Fifty percent of the possible objects hybridized to two probes will contribute to the

[66] K. Taneja and R. H. Singer, *Anal. Biochem.* **166,** 389 (1987).

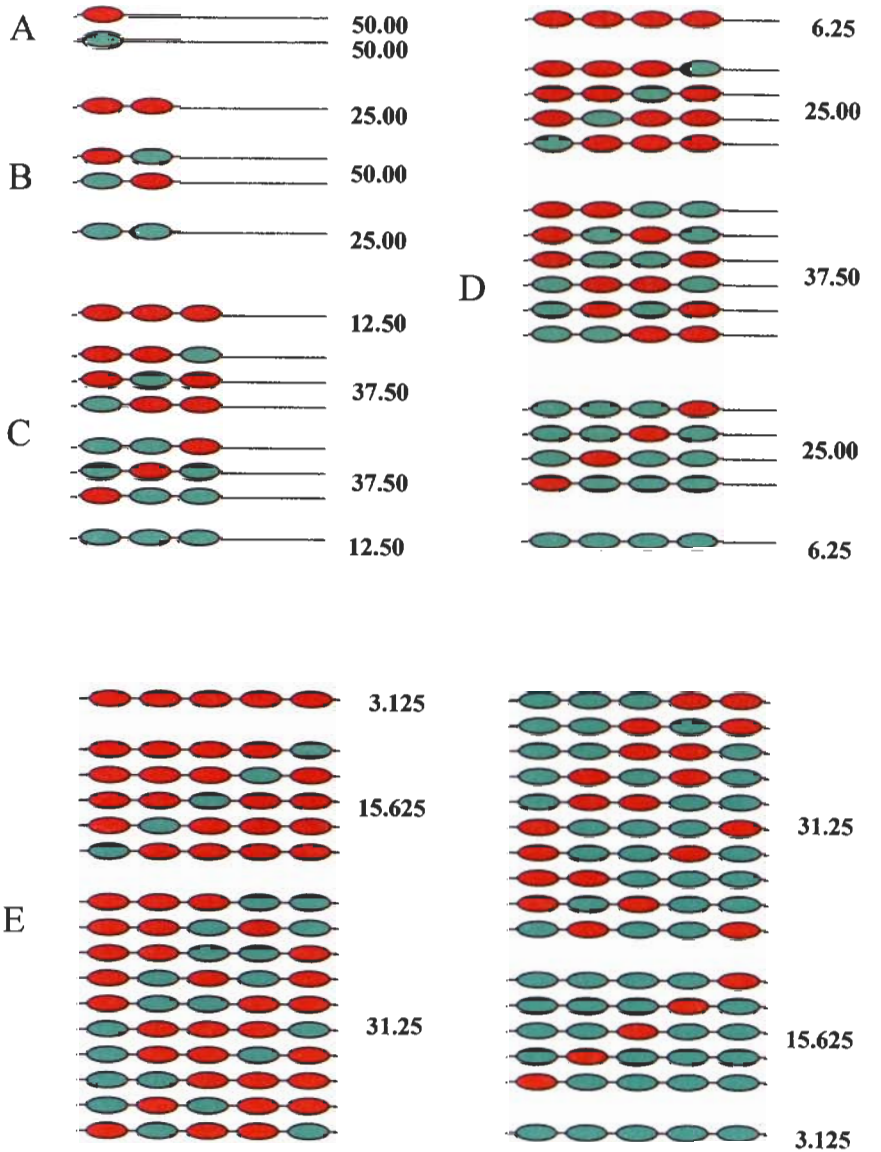

FIG. 22. A diagrammatic representation of the probability distribution of a 50 : 50 mixture of CY3- (red) and FITC- (green) labeled probes hybridized to the available sites on the 3′-UTR of β-actin mRNA. (A) The mRNA molecules that have only one site available will hybridize either a CY3- or a FITC-labeled probe. Therefore, there will be one-half as many objects in the respective image hybridized with one CY3 probe. (B) Molecules with two sites available have a 50% chance of hybridizing one CY3- and one FITC-labeled probe, but only a 25% chance of hybridizing two CY3 probes. Therefore, the number of objects hybridizing two CY3-labeled probes drops dramatically, whereas there is a concomitant contribution to the pool of observed objects hybridized to one CY3 probe. (C–E) Molecules with three, four, and five sites available will retain only 12.5, 6.25, and 3.125% of those sites exclusively hybridized to CY3. Therefore objects hybridized to three, four, and five CY3 probes become scarce.

objects that are categorized as hybridizing one CY3 probe. These will add to the apparent number of objects hybridizing one probe as detected in the CY3 channel. The other possible hybridization configurations, occurring for three, four, and five available sites, also contribute to the objects that are categorized as hybridizing one CY3 probe. The absolute number of objects contributed to the "one probe hybridized" category is small because there are fewer mRNA molecules that have three to five target sequences available. The overall result in the CY3 image is an apparent increase in the number of objects representing one hybridized probe molecule and an apparent diminishing of objects representing two to five probes hybridized.

A distribution of objects can be predicted quite accurately for a 50 : 50 mixture of probes. The respective probabilities of hybridization shown in the diagram can be used to calculate a hypothetical distribution based on the number of objects typically found in each category (one to five probes hybridized) of a cell hybridized with 100% CY3 probes (Table VII).

How do the statistics support single molecule detection? The TFI pattern of objects in the competed hybridization conforms to statistical prediction. Therefore the unit TFI that is used to identify an object hybridized to a single probe must indeed be the correct intensity for one probe. In turn, an object that hybridizes only one probe can only be one molecule. Objects that hybridize more than one

TABLE VII
STATISTICAL DISTRIBUTIONS OF HYBRIDIZED CY3 PROBES PREDICTED IN COMPETED HYBRIDIZATION[a]

Number of probes hybridized	100% CY3 probe	50% CY3, 50% FITC	
		Predicted	Actual
1	184	218	201
2	154	100	108
3	84	35	30
4	49	9	8
5	42	1.3	2

[a] A typical distribution of objects in a cell hybridized with 100% CY3-labeled probes, column 2, provides a profile of the available sites on each 3′-UTR of β-actin mRNA *in situ*. The probability distribution of a 50 : 50 mixture of CY3 and FITC-labeled probes (Fig. 22) is applied to the available sites and results in a "predicted" distribution of objects, column 3. A typical distribution of objects in a cell hybridized with a 50 : 50 mixture of CY3 and FITC probes, column 4, appears equal to the predicted distribution. A χ^2 test for the equality of distributions between two populations confirms that the "predicted" and "actual" distributions are equal. $\chi^2 = 1.301$, $\chi^2_{0.05} = 9.488$, df $= 4$.

probe, however, must also conform to the constrained spatial dimensions of one molecule to be unequivocally identified as one molecule.

Dual-Wavelength Hybridization to Resolve Intramolecular Distances as Close as 108 nm in Single Molecules of β-Actin mRNA

The objects detected in the FITC channel follow the same probability distribution pattern as those described for CY3 objects (Fig. 22). The competed hybridization diminishes the respective FITC signals compared to that of hybridization with 100% FITC-labeled probes.

Examination of the FITC image overlaid onto the CY3 image provides additional supporting evidence of single molecule detection of β-actin mRNA. The dual-wavelength image is zoomed in to focus on individual objects representing single molecules of β-actin mRNA (Fig. 23; Table VIII). Objects hybridized to two or three probes that also include both a CY3- and a FITC-labeled probe are selected. The probes show colocalization either through exact overlap of the respective maximal voxels associated with each spectrally distinct signal or through adjacent positioning of the respective maximal voxels. Both types of colocalization are expected if the object represents a single molecule of β-actin mRNA due to the fact that the set of five probes targeted to the 3′-UTR region is spaced relative to each other as close as 4 nucleotides and as distant as 360 nucleotides (Fig. 13).[2] The FITC and CY3 probes will show overlap colocalization when the hybridized

TABLE VIII
CYTOPLASMIC OBJECTS A, B, AND C AS SINGLE MOLECULES OF β-ACTIN mRNA[a]

Object	Fluorochrome	Object size (voxels)	TFI	Probes hybridized	Maximum voxel (TFI)	x, y, z
A	CY3	4	11630	1	4797	91, 199, 3
	FITC	5	3732	1	1191	91, 199, 3
B	CY3	3	16976	2	9727	98, 103, 11
	FITC	3	3066	1	1022	99, 103, 12
C	CY3	3	9747	1	4895	68, 136, 7
	FITC	3	3437	1	1866	69, 136, 8

[a] A 50 : 50 mixture of CY3 (red) and FITC (green)-labeled probes was hybridized to the available sites on the 3′-UTR of β-actin mRNA *in situ*. β-Actin mRNA may hybridize up to five 3′-UTR probes with one, two, or three the most probable number expected. Objects A, B, and C (from Fig. 23) have hybridized 2, 3, and 2 probes, respectively. The maximum voxels of the red and green components are within the expected linear constraints of the target 3′-UTR region. The TFI, the size of the respective red and green objects, and their distance apart confirm the hybridization to a single molecule of β-actin mRNA.

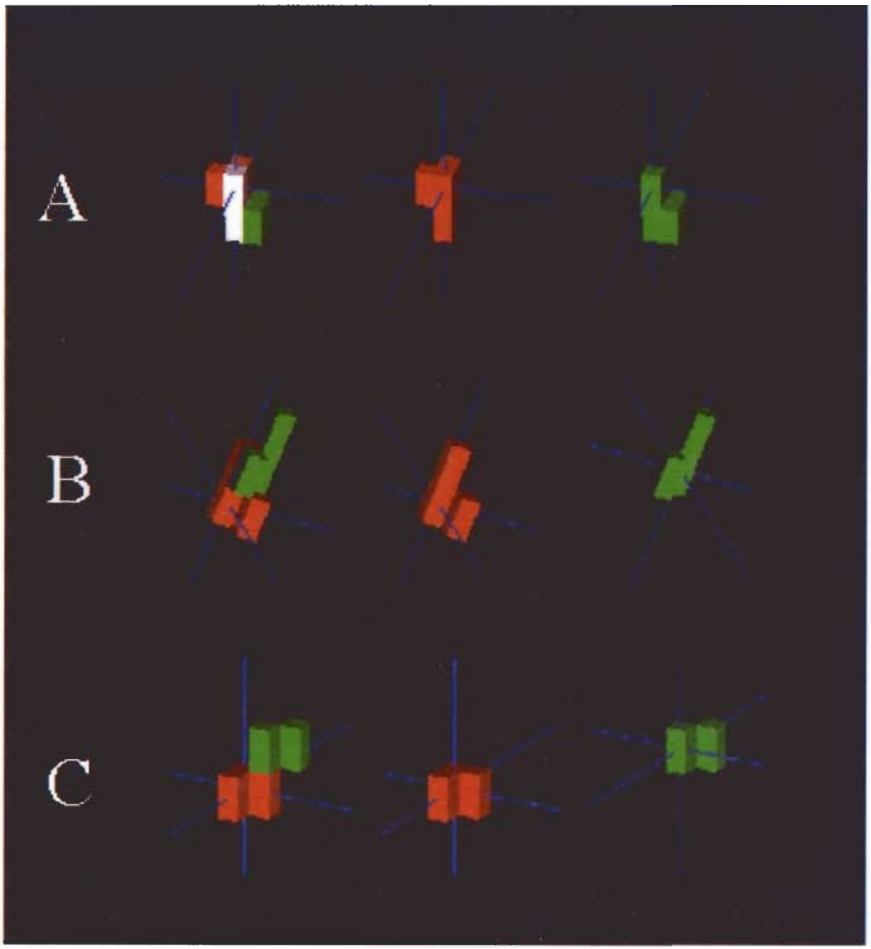

FIG. 23. Representative examples of β-actin mRNA that have simultaneously hybridized CY3 and FITC probes are shown zoomed in. The position of the maximum voxel for the respective CY3 and FITC objects is designated with a cross hair. The maximum voxel is the location of the point source (hybridized probe). (A) One CY3 (red) and one FITC (green) probe, same voxel colocalization (white). (B) Two CY3 probes and one FITC probe, adjacent voxel colocalization. (C) One CY3 and one FITC probe, adjacent voxel colocalization. Detailed data are provided for each object in Table VIII.

probes are linearly separated by 4 nucleotides, but will very likely be located in adjacent voxels when separated by 360 nucleotides (108 nm). Probes that are hybridized to separate molecules of mRNA would not be constrained to overlap or adjacent voxel colocalization (Fig. 24A). Therefore the colocalization as well as stoichiometry strongly supports single molecule detection of β-actin mRNA.

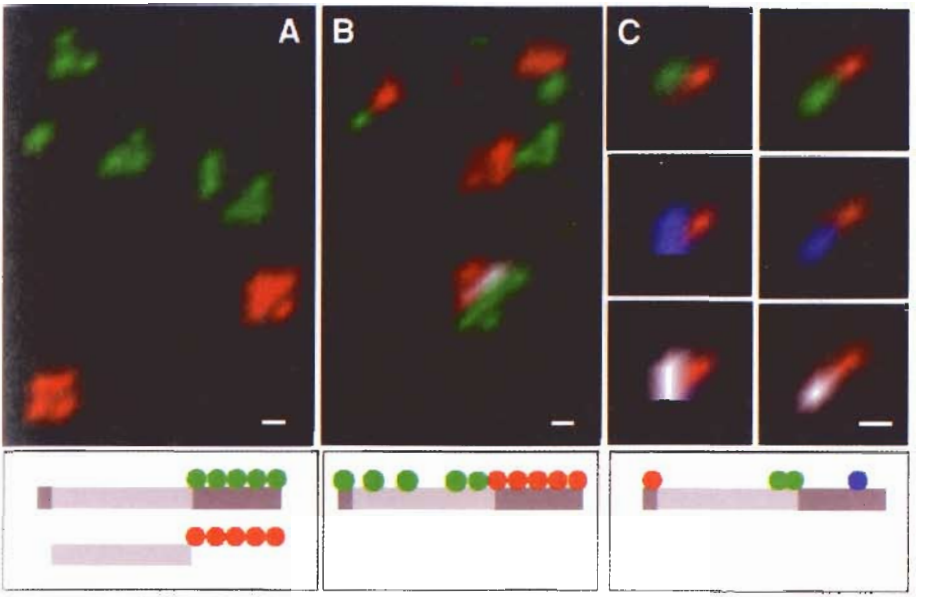

FIG. 24. Probing of intermolecular and intramolecular targets in the cytoplasm. (A) The detection of trans sequences. Both β- (green) and γ- (red) actin mRNA were detected simultaneously in the same cell with probes to their respective 3′-UTRs. Individual β- and γ-actin mRNAs segregate independently in the cytoplasm. [Statistical analysis of the frequency of measured separation distances in voxels (vo) (1 vo = 93 nm by 93 nm by 100 nm) between the red and the nearest green signal is expressed as cumulative percent: 0 vo = 0.1%, 1 vo = 1.5%, 2 vo = 6.4%, 3 vo = 13.7%, 4 vo = 25.1%, 5 vo = 36.5%; n (red) = 685, n (green) = 459.] (B) The detection of cis sequences. Two intramolecular regions of β-actin mRNA are resolved with five different probes targeted to the 3′-UTR (red) or the splice junction (SJ) sites (green). β-Actin mRNA molecules show nearest neighbor association of the 3′-UTR and the coding region. Frequency of separation distances in voxels: 0 vo = 2.4%, 1 vo = 15.8%, 2 vo = 32.9%, 3 vo = 59.1%, 4 vo = 72.6%, 5 vo = 87.2%; n (red) = 164, n (green) = 314. The 3′-UTR probes (red) are used to specifically detect β-actin mRNA. The SJ probes for β-actin (green) have homology with γ-actin, accounting for more green than red signal. Respective red and green pairs had TFI values consistent with single β-actin mRNA molecules. (C) Intramolecular measurement with three spectally distinct probes hybridized to two β-actin mRNAs. Two regions 631 bases (190 nm) apart were not resolved (CY5, blue; FITC, green); a third region, 1648 bases away (500 nm), was resolved (CY3, red). The colocalized voxels of the blue and green images are turned white. The distance between red and blue maxima is estimated to be 487 nm, consistent with a linear RNA. The schematic depicts the locations of the probes. Bar: 93 nm (A, B); 187 nm (C). Reprinted with permission from A. M. Femino, F. S. Fay, K. Fogarty, and R. H. Singer, *Science* **280,** 585 (1998). Copyright © 1998 American Association for the Advancement of Science.

Conclusion

Point sources of light emitting from fluorescent probes hybridized to molecular targets *in situ* are the basic units of information comprising a fluorescence digital image. Probes that conform as closely as possible to a point source maximize

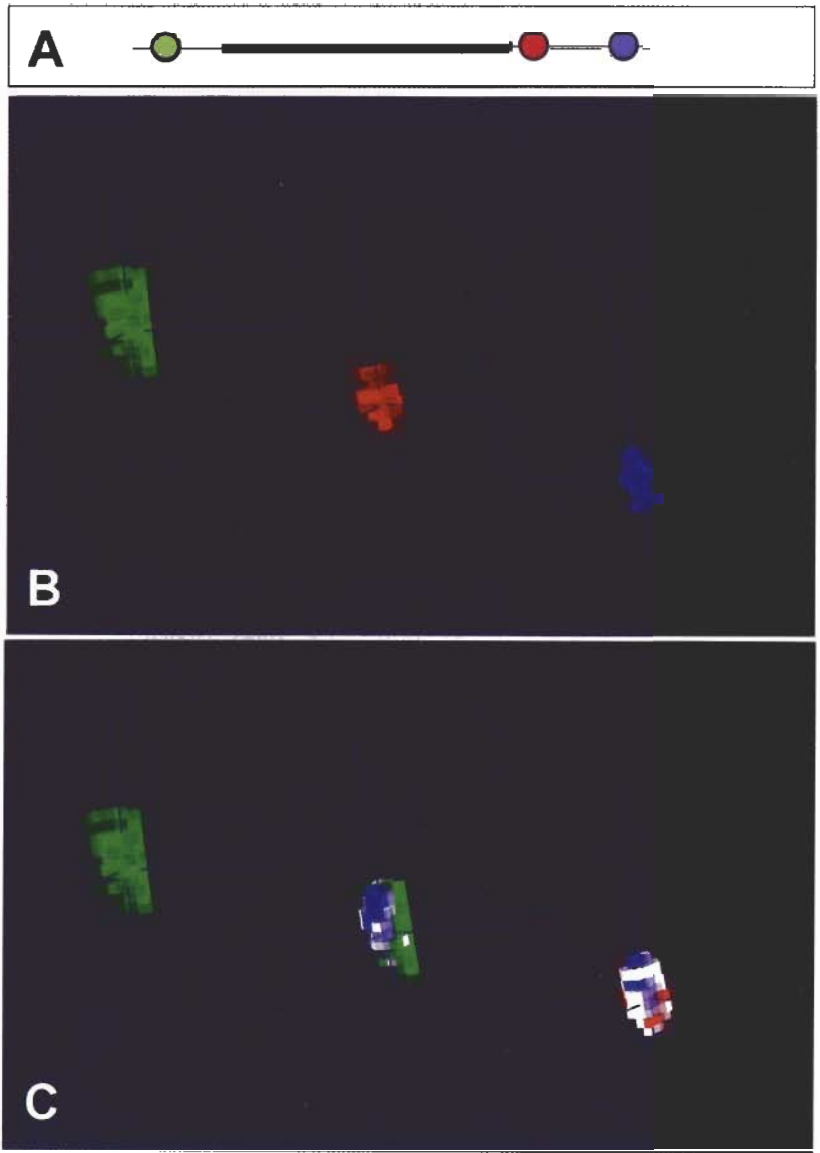

FIG. 25. A single β-actin transcription site is simultaneously detected with three probes targeted to the RNA, each labeled with a different fluorochrome. (A) A diagram of three spectrally distinct probes targeted to β-actin RNA. (B) The spatial distribution of signal from the probe targeted to the 5′-UTR (green) is expected to traverse the length of the gene during the peak of transcription at 15 min after serum induction. As expected, the signal appears to have the greatest spatial extent. The total number of green probes equals the total number of nascent RNA $= 26$. The spatial distribution of signal from both the proximal (14 probes) and the distal (8 probes) 3′-UTR is more condensed. (C) The signals from probes targeted to the proximal (red) and distal (blue) 3′-UTR are colocalized. Their respective spatial distributions are polarized toward one end of the 5′-UTR (green) signal. The interpretation is that the 5′ end of a transcribing β-actin gene can be resolved from the 3′ end.

analysis potential. Knowledge about image formation theory encourages a better appreciation for hybridization probe design.

The limitations of optical microscopy are reviewed to emphasize the necessity for optical sectioning and rigorous deconvolution. Deconvolution restores the TFI of an object to a delimited volume that is amenable to analysis for quantitative and spatial information. However, image formation theory, image processing, and deconvolution algorithms do not provide a solution to identify hybridization targets in an image. They do, however, provide a very important foundation for such a solution.

Definitive analysis of the fluorescence distribution in an image in terms of single molecules requires the identification of probe hybridization sites. Probes that approach the infinitely small spatial dimension of a point source and have a good *S/N* ratio are optimal for providing accurate spatial information about their respective targets and accurate intensity information to determine copy number following image deconvolution.

To accomplish a definitive analysis for an FISH experiment, a methodology was devised to calibrate oligonucleotide probes under imaging conditions. The calibration of the total fluorescence intensity attributed to a theoretical deconvolved single probe molecule led to the definitive identification of point sources that represented true hybridization sites in a deconvolved image. With adequate digital camera sensitivity and *S/N* ratio, it can be shown that many fluorescent objects represent single fluorescent probes hybridized to single target molecules

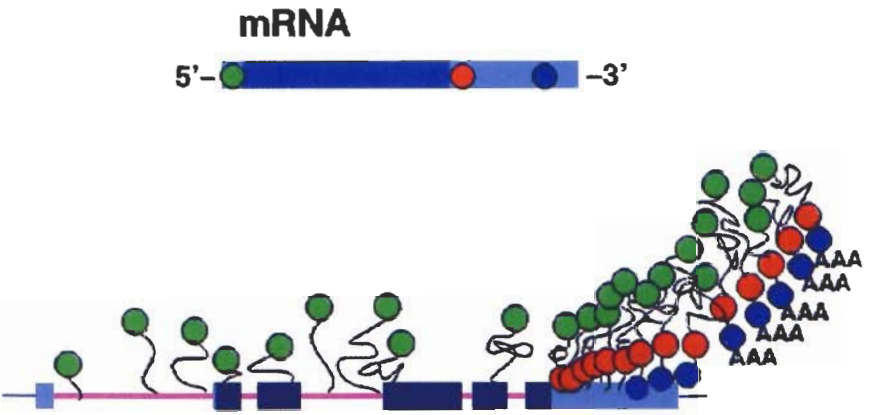

FIG. 26. A dynamic profile of transcription at one β-actin allele resolved with three spectrally distinct probes. The 5′-UTR probe detects all the nascent RNA (green). A second probe detects RNA that has progressed beyond the first 50 bases of the 3′-UTR (red), and the third probe detects RNA that has progressed to the distal region of the 3′-UTR (blue). The triple As indicate transcripts beyond the polyadenylation site. Reprinted with permission from A. M. Femino, F. S. Fay, K. Fogarty, and R. H. Singer, *Science* **280,** 585 (1998). Copyright © 1998 American Association for the Advancement of Science.

and, as a result, single copies of mRNA were detected and identified in the cytoplasm and nucleus of individual cultured cells.

Analysis of point sources representing one hybridized probe has provided additional information concerning the nature of the imaging process. The pixel does not suffice as the unit for analysis of a digital image involving fluorescence *in situ* hybridization. The unit for analysis is redefined to be the TFI of one probe molecule that has spatial dimensions, and is visualized as a three-dimensional cluster of contiguous voxels that varies in size and shape. The shape and size of a point source, representing one hybridized probe, contains information about the subpixel location of the point source.

The detailed characterization of biological molecules *in situ* is now possible using FISH. Unprecedented detail can be revealed from a hybridized cell that has been interrogated with carefully engineered, quantitatively accurate probes, followed by three-dimensional imaging and deconvolution.

The quantitative and spatial accuracy that results from the described analytical process provides a new and powerful visualization of biological events at the single molecule level. In addition to proving that single molecules could be visualized using epifluorescence microscopy, intramolecular spatial resolution, within one mRNA molecule, was demonstrated *in situ* (Figs. 23 and 24B and C). Additional experimental results demonstrated new detailed biological information concerning RNA processing at transcription sites as a consequence of accurate counting of the number of nascent RNA molecules at specific regions along the actin gene (Figs. 25 and 26).[2,3] The technology increases the potential of the FISH technique and dramatically extends the resolution limits of fluorescence light microscopy.

[14] Single Ion Channel Imaging

By ALOIS SONNLEITNER and EHUD ISACOFF

Introduction

Single-channel ionic current recording with the patch clamp, and by reconstitution into artificial lipid bilayers, greatly enhanced the understanding of ion channels by providing a direct view of the conductance and gating dynamics of channels. Here we describe an optical analog to the patch clamp that reveals protein motions on the single-channel level. Functional transitions that cannot be detected directly in ionic current recordings, because they do not open and close the channel gates, can be detected optically. We apply the method to a voltage-gated K^+ channel to detect the activation rearrangements of the voltage sensor that precede opening.

0076-6879/03 $35.00